Dear Editor,

Thank you for accepting our work. As per your suggestions, I have addressed all your comments.

A point by point reply to the comments is provided below.

Sincerely,

Sreeush M. G.

Reply to the editor comments:

1. Line 158 U and W are the velocity (please add W as in the equations below)

   Corrected accordingly. Please refer lines 158 and 172 of the revised manuscript.

2. Lines 188-189: I would say "Inorganic phosphorus"

   Corrected accordingly. Please see lines 188 -189 in the revised manuscript.

3. Line 203 : how Jprod can give a new-production in gC/m2/yr ? you need to have a conversion factor from phosphorus to carbon.

   Using the Redfield ratio $R_{C:P}$ = 117:1. The phosphorus is converted into carbon. Please refer lines 202 – 203 in the revised manuscript.

4. Line 283 : why did you mention ("see Appendix B") ? Figure 2 is not in the appendix

   Appendix B explains the method of calculating average relative photosynthesis shown in figure 2. Please refer the lines 282 – 283 of the revised manuscript.

5. Lines 330-331 : the order of presentation of case study is first SC and then SCTR.

   Corrected accordingly. Please refer lines 328 – 331 of the revised manuscript.

Biological Production in the Indian Ocean Upwelling Zones, Part – I: Refined Estimation via the Use of a Variable Compensation Depth in Ocean Carbon Models

Mohanan Geethalekshmi Sreeush[1,2,*].

Vinu Valsala[1],

Sreenivas Pentakota[1],

Koneru Venkata Siva Rama Prasad[2],

Raghu Murtugudde[3]

[1]Indian Institute of Tropical Meteorology, Pune, India

[2]Department of Meteorology and Oceanography, Andhra University, India

[3]ESSIC, University of Maryland, USA

(*Under revision BGD*)

*Corresponding author address:
Indian Institute of Tropical Meteorology,
Dr. Homi Bhabha Road, Pashan, Pune 411 008, India
E-Mail: sreeushmg@tropmet.res.in

Abstract

Biological modeling approach adopted by the Ocean Carbon-cycle Model Inter-comparison Project (OCMIP-II) provided amazingly simple but surprisingly accurate rendition of the annual mean carbon cycle for the global ocean. Nonetheless, OCMIP models are known to have seasonal biases which are typically attributed to their bulk parameterization of 'compensation depth'. Utilizing the criteria of surface Chl-a based attenuation of solar radiation and the minimum solar radiation required for production, we have proposed a new parameterization for a spatially and temporally varying 'compensation depth' which captures the seasonality in the production zone reasonably well. This new parameterization is shown to improve the seasonality of CO_2 fluxes, surface ocean pCO_2, biological export and new production in the major upwelling zones of the Indian Ocean. The seasonally varying compensation depth enriches the nutrient concentration in the upper ocean yielding more faithful biological exports which in turn leads to an accurate seasonality in the carbon cycle. The export production strengthens by ~70% over the western Arabian Sea during monsoon period and achieves a good balance between export and new production in the model. This underscores the importance of having a seasonal balance in model export and new productions for a better representation of the seasonality of carbon cycle over upwelling regions. The study also implies that both the biological and solubility pumps play an important role in the Indian Ocean upwelling zones.

Keywords: Indian Ocean upwelling zones, Carbon cycle, Seasonal cycle - CO_2 flux and Oceanic pCO_2, Biogeochemical model parameterization, Export production - New production balance, Solubility and Biological pump.

1. Introduction

The Indian Ocean is characterized by the unique seasonally reversing monsoon wind systems which act as the major physical drivers for the coastal and open ocean upwelling processes. The major upwelling systems in the Indian Ocean are (1) the western Arabian Sea (WAS; Ryther and Menzel, 1965; Smith et al., 2001; Sarma, 2004; Wiggert et al., 2005, 2006; Murtugudde et al., 2007; McCreary et al., 2009; Prasanna Kumar et al., 2010; Naqvi et al., 2010; Roxy et al., 2015) (2) the Sri Lanka Dome (SLD; Vinayachandran et al., 1998, 2004), (3) Java and Sumatra coasts (SC; Murtugudde et al., 1999a; Susanto et al., 2001; Osawa et al., 2010; Xing et al., 2012) and (4) the Seychelles-Chagos thermocline ridge (SCTR; Murtugudde et al., 1999b; Dilmahamod et al., 2016, Figure 1). The physical and biological processes and their variability over these key regions are inseparably tied to the strength of the monsoon winds and associated nutrient dynamics. The production and its variability over these coastal upwelling systems are a key concern for the fishing community, since they affect the day-to-day livelihood of the coastal populations (Harvell et al., 1999; Roxy et al., 2015; Praveen et al., 2016) and are important for the Indian Ocean rim countries due to their developing country status.

Arabian Sea is a highly productive coastal upwelling system characterized by phytoplankton blooms both in summer (Prasanna Kumar et al., 2001; Naqvi et al., 2003; Wiggert et al., 2005) and winter (Banse and McClain, 1986; Wiggert et al., 2000; Barber et al., 2001; Prasannakumar et al., 2001; Sarma, 2004). The Arabian Sea is known for the second largest Tuna fishing region in the Indian Ocean (Lee et al., 2005). The Somali and Omani upwelling regions experience phytoplankton blooms that are prominent with Net Primary Production (NPP) exceeding 435 g C m^{-2} yr^{-1} (Liao et al., 2016). On the other hand productivity over the SLD (Vinayachandran and Yamagata, 1998) is triggered by open ocean Ekman suction with strong Chl-a blooms during the

summer monsoon (Murtugudde et al., 1999a; Vinayachandran et al., 2004). Similarly, the SC upwelling is basically due to the strong alongshore winds and its variation is associated with the impact of equatorial and coastal Kelvin waves (Murtugudde et al., 2000, Valsala and Rao, 2016). The interannual variability associated with the Java-Sumatra coastal upwelling is strongly coupled with ENSO (ElNiño Southern Oscillation) through the Walker cell and Indonesian throughflow (Susanto et al., 2001; Valsala et al., 2011) and peaks in July through August with a potential new production of 0.1 Pg C yr^{-1} (Xing et al., 2012). The SCTR productivity has a large spatial and interannual variability. The warmer upper ocean condition associated with El Niño reduces the amplitude of subseasonal SST variability over the SCTR (Jung and Kirtman., 2016). The Chl-a concentration peaks in summer when the southeast trade winds induce mixing and initiate the upwelling of nutrient-rich water (Murtugudde et al., 1999a; Wiggert et al., 2006; Vialard et al., 2009; Dilmahamod et al., 2016).

Understanding the biological production and variability in the upwelling systems is important because it gives us crucial information regarding marine ecosystem variability (Colwell, 1996; Harvell et al., 1999). The observations also provide vital insights into physical and biological interactions of the ecosystem (Naqvi et al., 2010) as well as the biophysical feedbacks (Murtugudde et al., 1999a), although limitations of sparse observations often force us to depend on models to examine the large spatio-temporal variability of the ecosystem (Valsala et al., 2013). Simple to intermediate complexity marine ecosystem models have been employed by several of the previous studies (Sarmiento et al., 2000; Orr et al., 2001; Matsumoto et al., 2008). However, the representation of marine ecosystem with proper parameterizations in models has always been a daunting task. This is an impediment to the accurate representation of biological

primary and export productions in models (Friedrichs et al., 2006, 2007) and these issues also impact the modeling of upper trophic levels (Lehodey et al., 2010).

Biological production can be quantified with a better understanding of primary production which depends on water temperature, light and nutrient availability (Brock et al., 1993; Moisan et al., 2002) and this became the key reason for parameterizing the production in models as one or more combinations of these terms (Yamanaka et al., 2004). Any of these basic parameters can be tweaked to alter production in models. For example, the availability of nutrients and light determines the phytoplankton growth (Eppely et al., 1972) or growth rate (Boyd et al., 2013). Stoichiometry and carbon-to-Chl-a ratios are other important factors to be considered in modeling (Christian et al., 2001, Wang et al., 2009) but we will not consider them in this study.

The Ocean Carbon-cycle Model Intercomparison Project (OCMIP) greatly improved our understanding of global carbon cycle (Najjar and Orr, 1998). OCMIP-II further introduced a simple phosphate-dependent production term in biological models for long-term simulations of the carbon cycle in response to anthropogenic climate change with an accurate annual mean state (Najjar and Orr, 1998; Orr et al., 2001; Doney et al., 2004). However, the OCMIP – II model simulations come with a penalty of strong seasonal biases when compared with observations (Orr et al., 2003). In this protocol, the community compensation depth (hereafter Zc) is defined as the depth at which photosynthesis equals entire community respiration and the irradiance at which this balance achieved is the compensation irradiance (E_{com}). Note that Zc is clearly different from the conventional euphotic zone depth (Morel, 1988). Within Zc, the production of organic phosphorous representing the biological production (in the present context the Net Community Production; NCP) is given as $J_{prod} = \frac{1}{\tau}([PO_4] - [PO_4^*])$, where $[PO_4]$ is the model phosphate concentration and $[PO_4^*]$ is observational phosphate concentration. τ is the restoration

timescale assumed to be 30 days. Whenever the model phosphate exceeds the observational phosphate, it allows production. At Zc, the NCP is zero and above Zc the Net Primary Production (NPP) exceeds the community respiration and the ecosystem will grow (Smetacek and Passow, 1990; Gattuso et al., 2006; Sarmiento and Gruber, 2006; Regaudix-de-Gioux and Duarte, 2010; Marra et al., 2014). However, Zc was held constant in time and space in OCMIP-II models (Najjar and Orr, 1998; Matsumoto et al., 2008) because the OCMIP-II protocol takes a minimalistic approach to biology and simplifies the model calculations with a very limited set of state variables suitable for long term simulations when implemented in coarse resolution models (Orr et al., 2005). However, in reality Zc varies in space and time (Najjar and Keeling, 1997) just as the euphotic zone depth does as documented in ship measurements (Qasim, 1977, 1982). The variation in Zc indicates the seasonality of the production zone itself.

Most of the biophysical models prescribe a constant value for Zc, e.g., a default value of Zc = 75 m in OCMIP –II protocol (Najjar and Orr, 1998) and Zc = 100 m in Minnesota Earth System Model (Matsumoto et al., 2008). Depending on the latitude, Zc varies between 50m and 100m in the real world (Najjar and Keeling, 1997). In our study we have attempted a novel biological parameterization scheme for spatially and temporally varying Zc in the OCMIP–II framework by representing the production as a function of solar radiation (Parsons et al., 1984) and prescribed Chl-a. In this hypothesis, a spatially and temporally varying Zc is estimated from the vertical attenuation of insolation by the surface Chl-a. The depth at which the insolation reaches the compensation irradiance (chosen as 10 Wm^{-2}) is taken as Zc. Phosphorous is the basic currency which limits the production within this varying Zc. This spatially and temporally varying Zc represents the seasonality in the production zone which is lacking in the original OCMIP-II protocol.

Regions of sustained upwelling like the eastern equatorial Pacific are well understood in terms of the role of upwelling in increasing the surface water pCO_2 to drive an outgassing of CO_2 into the atmosphere (Feely et al., 2001; Valsala et al., 2014). The Indian Ocean on the other hand experiences only seasonal upwelling which is relatively weak in the deep tropics but stronger off the coasts of Somalia and Oman and in the SLD (Valsala et al., 2013). The relative importance of the solubility vs. biological pump is not well understood. Our focus here on implementing seasonality in Zc of OCMIP models nonetheless leads to new insights on the impact of improved biological production on surface water pCO_2 and air-sea CO_2 fluxes. The improvements due to the effect of a variable Zc over the Indian Ocean and the sensitivity experiments where upwelling is muted strongly imply that the biological pump may play as much of a role as the solubility pump in determining surface pCO_2 and CO_2 fluxes over the Indian Ocean.

The paper is organized as follows. Model, Data, and Methods are detailed in Section 2. The spatially inhomogeneous Zc derived with the new parameterization and its impact on simulated seasonality of biology and carbon cycle are detailed in Section 3. Further a conclusion is provided in Section 4.

2. Model, Data, and Methods

2.1. Model

The study utilizes the Offline Ocean Tracer Transport Model (OTTM; Valsala et al., 2008) coupled with OCMIP biogeochemistry model (Najjar and Orr, 1998). OTTM does not compute currents and stratifications (i.e., temperature and salinity) on its own. It is capable of accepting any ocean model or data-assimilated product as physical drivers. The physical drivers prescribed

include 4-dimensional currents (U, V, W), temperature, salinity, and 3-dimensional mixed layer depth, surface freshwater and heat fluxes, surface wind stress and sea surface height. The resolution of the model setup is similar to the parent model from which it borrows the physical drivers. With the given input of Geophysical Fluid Dynamics Laboratory (GFDL) reanalysis data (Chang et. al., 2012), the zonal and meridional resolutions are 1^{o} with 360 grid points longitudinally and 1^{o} at higher latitudes but having a finer resolution of 0.8^{o} in the tropics, with 200 latitudinal grid points. The model has 50 vertical levels with 10m increment in the upper 225m and stretched vertical levels below 225m. The horizontal grids are formulated in spherical coordinates and vertical grids are in z levels. The model employs a B-grid structure in which the velocities are resolved at corners of the tracer grids. The model uses a centered-in-space and centered-in-time (CSCT) numerical scheme along with an Asselin-Robert filter (Asselin, 1972) to control the ripples in CSCT.

The tracer concentration (C) evolves with time as

$$\frac{\partial C}{\partial t} + U.\nabla_H C + W\frac{\partial C}{\partial z} = \frac{\partial}{\partial z}K_z\frac{\partial}{\partial z}C + \nabla_H.(K_h\nabla_H C) + J + F \qquad (1)$$

where ∇_H is the horizontal gradient operator, U and W are the horizontal and vertical velocities respectively. K_z is the vertical mixing coefficient, and K_h is the two-dimensional diffusion tensor. J represents any sink or source due to the internal consumption or production of the tracer. F represents the emission or absorption of fluxes at the ocean surface. Here, the source and sink terms are provided through the biogeochemical model. Vertical mixing is resolved in the model using K- profile parameterization (KPP; Large et al., 1994).

In addition to KPP, the model uses a background vertical diffusion reported by Bryan and Lewis (Bryan and Lewis, 1979). For horizontal mixing, model incorporates Redi fluxes (Redi, 1982)

and GM fluxes (Gent and Mcwilliams, 1990) which represent the eddy-induced variance in the mean tracer transport. A weak Laplacian diffusion is also included in the model for computational stability where the sharp gradient in concentration occurs.

2.2. Biogeochemical model

The biogeochemical model used in the study is based on the OCMIP – II protocol as stated above. The main motivation of OCMIP–II protocol is to employ a minimalistic approach to simulate the ocean carbon cycle with a nutrient restoration approach to calculate the oceanic biological production (Najjar et al., 1992; Anderson and Sarmiento, 1995). The present version of the model has four prognostic variables coupled with the circulation field, viz., inorganic phosphorus (PO_4^{3-}), dissolved organic phosphorus (DOP), dissolved inorganic carbon (DIC) and alkalinity (ALK). The basic currency for the biological model is phosphorous because of the availability of a more extensive phosphate database and to eliminate the complexities associated with nitrogen fixation and denitrification. Detailed model equations and variables are provided in Appendix-A with only a brief description given below.

The production of organic phosphorus in the model using the nutrient restoring approach is given by

$$J_{prod} = \frac{1}{\tau}([PO_4] - [PO_4]^*) \quad (2)$$

$$[PO_4] > [PO_4]^* \; ; Z < Zc$$

$$J_{prod} = 0 \quad (3)$$

$$[PO_4] \leq [PO_4]^*$$

Where J_{prod} represents the biogeochemical flows with respect to production of organic phosphorous. $[PO_4]^*$ is the observed phosphate concentration and τ=30 days is the restoration time scale (Najjar et. al., 1992). The conversion of phosphorus to carbon is done by multiplying Redfield ratio ($R_{C:P}$= 117).

The vertically integrated new production (g C m^{-2} yr^{-1}) in the model is defined as

$$New\ production = \int_{zc}^{0} -J_{prod}\ dz \qquad (4)$$

The export production (g C m^{-2} yr^{-1}) in the model is calculated as

$$Export\ production = (1-\sigma)\int_{0}^{zc} J_{prod}\ dz \qquad (5)$$

Air-sea CO_2 flux in the model is estimated by,

$$F = K_w\ \Delta\ pCO_2 \qquad (6)$$

where K_w is gas transfer velocity and $\Delta\ pCO_2$ is the difference in partial pressure of carbon dioxide between the ocean and atmosphere.

pCO_2 is calculated in the model by using DIC and ALK and is given by,

$$pCO_2 = \frac{[DIC]}{K_0}\frac{[H^+]^2}{[H^+]^2 + K_1[H^+] + K_1K_2} \qquad (7)$$

Where $[H^+]$ is calculated using Newton-Raphson iterative method (Press et. al., 1996, Najjar and Orr, 1998). K_0 is the solubility constant of CO_2 and K_1, K_2 are the dissociation constant for carbonic acid, respectively (Sarmiento and Gruber, 2006, Weiss, 1974, Mehrbach et al., 1973, Dickson and Millero, 1987, Najjar and Orr, 1998).

215 Details of all parameters in the biogeochemical model and calculations of solubility and
216 biological pump are listed in Appendix-A. The design and validation of the physical model is
217 reported by Valsala et al., (2008, 2010b) and biogeochemical model by Najjar and Orr (1998).

218

219 **2.3. Data**

220 For validating the model results, observational datasets of CO_2 flux and pCO_2 are taken
221 from Takahashi et al., (2009). Satellite-derived NPP data were taken from Sea-viewing Wide
222 Field of view Sensor (SeaWiFS) Chl-a product, calculated using Vertically Generalized
223 Production Model (VGPM; Behrenfeld and Falkowski, 1997). The NPP data is scaled to export
224 production (EP) by multiplying with an e-ratio (e = 0.37) representative of Indian Ocean
225 upwelling zones (Sarmiento and Gruber, 2006, Laws et al., 2000; Falkowski et al., 2003). The
226 initial conditions for PO_4 are taken from the World Ocean Atlas (Garcia et al., 2014). Initial
227 conditions for DIC and ALK are taken from the Global Ocean Data Analysis Project (GLODAP;
228 Key et al., 2004) dataset. The dissolved Organic Phosphorous (DOP) is initialized with a
229 constant value of 0.02 μmol kg^{-1} (Najjar and Orr, 1998). The data sources and citations are
230 provided in the Acknowledgement.

231

232 **2.4. Methods**

233 A spin-up for 50 years from the given initial conditions is performed with the
234 climatological physical drivers. As the initial conditions are provided from a mean state of
235 observed climatology, this duration of spin-up is sufficient to reach statistical equilibrium in the

upper 1000 m (Le Quere et al., 2000). Atmospheric pCO_2 has been set to a value from the 1950s in the spin-up run for calculating the air-sea CO_2 exchange. A seasonal cycle of atmospheric pCO_2 has been prescribed as in Keeling et al. (1995).

After the spin-up, an interannual simulation for 50 years from 1961 to 2010 has been carried out with the corresponding observed atmospheric pCO_2 described in Keeling et al., (1995). The first five years of the interannual run were looped five times through the physical fields of 1961 repeatedly for a smooth merging of the spin-up restart to the interannual physical variables. Since the study is focused on bias corrections to the seasonal cycle of pCO_2 and DIC with a variable Zc, a model climatology for carbon cycle has been constructed from 1990 to 2010, which includes the anthropogenic increase of oceanic DIC in the climatological calculation and is comparable with the Takahashi et al. (2009) observations.

Additional two sensitivity experiments have been performed separately by providing annual mean currents or temperatures as drivers over selected regions of the basin in order to segregate the role of varying Zc in improving the seasonality of carbon cycle. The aim of these sensitivity experiments is to understand how successful the new parameterization for Zc is in capturing the carbon cycle variability related to the upwelling episodes even though the seasonal cycle in physics is suppressed. The model driven with annual mean currents suppresses the effect of upwelling by muting the Ekman divergence over the region of interest. On the other hand, the model forced with annual mean temperatures suppresses the cooling effect of upwelling. A smoothing technique with linear interpolation($U = U(1 - x) + \bar{U}x$) is applied to the offline-data in order to blend the annual mean fields ($\bar{U}$) provided to the selected region with the rest of the domain (U) in order to reduce a sudden transition at the boundaries. Here x represents an index which varies between 0 and 1 within a distance of 10^0 from the boundaries of

259 the region of interest to the rest of the model domain. Results of sensitivity experiments are
260 provided in supplementary material.

261

262 **2.5. Community compensation depth (Zc) parameterization**

263 The OCMIP – II protocol separates the production and consumption zones by a depth termed
264 as compensation depth (Zc); the depth at which photosynthesis is large enough to balance the
265 community respiration (i.e., both the autotrophic and heterotrophic respiration). At the
266 community compensation depth, the NCP is zero i.e., NCP = NPP - R_h = 0, (i.e., NPP = GPP –
267 R_a), GPP is gross primary production, and R_h and Ra are the heterotrophic and autotrophic
268 respirations, respectively (Smetacek and Passow, 1990; Najjar and Orr, 1998; Gattuso et al.,
269 2006; Regaudix-de-Gioux and Duarte, 2010; Marra et al., 2014). The light intensity at Zc is
270 compensation irradiance (E_{com}), the irradiance at which the gross community primary production
271 balances respiratory carbon losses for the entire community (Gattuso et al., 2006; Regaudix-de-
272 Gioux and Duarte, 2010). We define a spatially and temporally varying compensation depth
273 (hereafter varZc) as a depth where compensation irradiance (attenuated by surface Chl-a, Jerlov
274 et al., 1976) reaches a minimum value of 10 W m^{-2}. In this way, the varZc has both spatio-
275 temporal variability of light as well as Chl-a. The Chl-a is given as monthly climatology as
276 constructed from satellite data. Observations show that the primary production reduces rapidly to
277 20% or less of the surface value below a threshold of 10 W m^{-2} (Parsons et al., 1984; Ryther,
278 1956; Sarmiento and Gruber, 2006). Moreover higher ocean temperatures (those in the tropics)
279 enhance the respiration rates resulting in high compensation irradiance (Parsons et al., 1984;
280 Ryther, 1956; Lopez-Urrutia et al., 2006; Regaudix-de-Gioux and Duarte, 2010). A study by

281 Regaudix-de-Gioux and Duarte (2010) reported the mean value of compensation irradiance over
282 the Arabian Sea as 0.4 ± 0.2 mol photon m^{-2} day^{-1} which is close to 10 W m^{-2} day^{-1}.

283 Figure 2 compares the scatter of average relative photosynthesis (See Appendix-B for
284 details) within varZc as a function of solar radiation for the Indian Ocean ~~(see Appendix B)~~. This
285 encapsulates the corresponding curve from the observations for the major phytoplankton species
286 in the ocean such as diatoms, green algae and dinoflagellates (Ryther et al., 1956; Parsons et al.,
287 1984; Sarmiento and Gruber, 2006). The model permits 100% production of organic phosphorus
288 for radiation above 10 W m^{-2}. However the availability of phosphate concentration in the model
289 acts as an additional limit for production which indirectly represents the photoinhibition at higher
290 irradiance; for example, in the oligotrophic gyres.

291

292 3. **Results and Discussions**

293 The inclusion of seasonality in Zc by way of parameterizing varZc leads to a remarkable
294 spatio-temporal variability in Zc (Figure 3). Zc over the Arabian Sea varies from 10 m to 25 m
295 during December to February (DJF) and deepens down to 45 m during March to May (MAM)
296 due to the increase in the surface solar radiation. During the monsoon season i.e., June to
297 September (JJAS), Zc again shoals to 10 m - 35 m due to the attenuation of solar radiation by the
298 increased biological production (Chl-a). During October to November (ON), Zc slightly deepens
299 as compared to JJAS.

300 The Bay of Bengal Zc deepens from 35 m to 40 m during DJF and further deepens to 50 m
301 during MAM when the solar radiation is maximum and biological production is minimum

(Prasannakumar et al., 2002). Further reduction of Zc can be seen through JJAS as a result of a reduction in solar radiation during monsoon cloud cover. Zc during ON is 35 m on average.

The equatorial Indian Ocean can be seen as a belt of 40 m - 45 m Zc throughout the season except for JJAS. During JJAS, a shallow Zc is seen near the coastal Arabian Sea (around 10 m to 35 m) presumably due to the coastal Chl-a blooms. Deep Zc off the coast of Sumatra (~ 40 m to 50 m) is found during JJAS. Java-Sumatra coastal upwelling is centered on SON (Susanto et al., 2001) and upwelling originates at around 100 m depth (Valsala and Maksyutov, 2010a; Xing et al., 2012).

Southward of 10^{o}S in the oligotrophic gyre region, Zc varies from 40 m to more than 60 m throughout the year. A conspicuous feature observed while parameterizing the solar radiation and Chl-a dependent Zc is that its maximum value never crosses 75 m especially in the Indian Ocean which is the value specified in OCMIP-II models. The cutoff depth of 75 m in OCMIP-II is obtained from observing the seasonal variance in oxygen data (Najjar and Keeling, 1997) as an indicator of the production zone. However, our results show that parameterizing a production zone based on solar radiation and Chl-a predicts a production zone and its variability that is largely less than 75 m. The relevance of varZc in the seasonality of the modeled carbon cycle is illustrated as follows.

3.1. Simulated seasonal cycle of pCO_2 and CO_2 fluxes

The annual mean biases in simulated CO_2 fluxes and pCO_2 were evaluated by comparing with Takahashi et al., (2009) observations (Figure 4). The model biases are significantly reduced

323 with the implementation of varZc compared to that of the constant Zc (hereinafter constZc). A
324 notable reduction in pCO_2 bias (by ~ 10µatm) is observed along the WAS (Figure 4d).

325 In order to address the role of the new biological parameterization of a variable Zc, we
326 zoom in on four key regions where the biological production and CO_2 fluxes are prominent in the
327 Indian Ocean with additional sensitivity experiments (see Introduction and references therein).
328 The regions (boxes shown in Figure 1) we considered are, (1) Western Arabian Sea (WAS;
329 40^oE:65^oE, 5^oS:25^oN) (2) Sri Lanka Dome (SLD; 81^oE:90^oE, 0^o:10^oN) and (3) Sumatra Coast
330 (SC; 90^oE:110^oE, 0^o:10^oS) (4) Seychelles-Chagos Thermocline Ridge (SCTR; 50^oE:80^oE,
331 5^oS:10^oS; Figure 1). The seasonal variations of Zc over these selected key regions are shown in
332 Figure 5. A detailed analysis of CO_2 fluxes, pCO_2, biological export and new productions and the
333 impact of varZc simulations in improving the strength of biological pump and solubility pump
334 for these key regions are presented below.

335

336 **3.2. Western Arabian Sea (WAS)**

337 The WAS Zc has a double peak pattern over the annual cycle. During the February-March
338 period, Zc deepens down to a maximum of 43.85 ± 2.3 m into March and then shoals to 25.75 ±
339 1.5 m (Figure 5) during the monsoon period (uncertainty represents the interannual standard
340 deviations of monthly data from 1990-2010). This shoaling of Zc depth during the monsoon
341 indicates the potential ability of the present biological parameterization to capture the wind-
342 driven upwelling related production in the WAS. During the post-monsoon period, the second
343 deepening of Zc occurs during November with a maximum depth of 34.91 ± 2.2 m. The ability to
344 represent the seasonality of the production zone renders a unique improvement in CO_2 flux

345 variability especially in the WAS in comparison to the OCMIP-II experiments (Orr et al, 2003;
346 Figure 6a).

347 OCMIP –II simulations with a constZc of 75 m underestimate the CO_2 flux when compared
348 to the observations of Takahashi et al. (2009). This underestimation is clearly visible during the
349 monsoon period. Our simulations with the varZc result in a better seasonality of CO_2 flux when
350 compared with Takahashi et al. (2009) observations (Figure 6a). The improvement due to the
351 varZc scheme is able to represent the seasonality of CO_2 flux better especially during the
352 monsoon period when wind-driven upwelling is dominant. Obviously, the relative role of the
353 biological and solubility pumps have to be deciphered in this context.

354 The CO_2 flux during July from observations, constZc, and varZc simulations are 3.09 mol m^{-2}
355 yr^{-1}, 1.82 ± 0.4 mol m^{-2} yr^{-1} and 3.10 ± 0.5 mol m^{-2} yr^{-1}, respectively. Southwesterly wind-driven
356 upwelling over the WAS especially off the Somali coast (Smith and Codispoti, 1980; Schott,
357 1983; Smith, 1984) and Oman (Bruce, 1974; Smith and Bottero, 1977; Swallow, 1984; Bauer et
358 al., 1991), pulls nutrient-rich subsurface waters closer to the surface while the available turbulent
359 energy due to the strong winds lead to mixed layer entrainment of the nutrients resulting in a
360 strong surface phytoplankton bloom (Krey and Babenerd, 1976; Banse, 1987; Bauer, 1991;
361 Brock et al, 1991). This regional bloom extends over 700 km offshore from the Omani coast due
362 to upward Ekman pumping driven by strong, positive wind-stress curl to the northwest of the low
363 level jet axis and the offshore advection (Bauer et al., 1991; Brock et al., 1991; Brock and
364 McClain, 1992a, b; Murtugudde and Busalacchi, 1999, Valsala, 2009) resulting in strong
365 outgassing of CO_2 flux and an enhanced pCO_2 in the WAS (Valsala and Maksyutov, 2013;
366 Sarma et al., 2002). The seasonal mean CO_2 flux during the southwest monsoon period (JJAS)
367 for constZc and varZc simulations are 1.44 ± 0.2 mol m^{-2} yr^{-1} and 2.31 ± 0.4 mol m^{-2} yr^{-1},

368 respectively. The biological parameterization of varZc considerably improves the average CO_2
369 flux during the monsoon period by 0.86 ± 0.1 mol m^{-2} yr^{-1}. The annual mean CO_2 flux from
370 observations, constZc and varZc simulations are 0.94 mol m^{-2} yr^{-1}, 0.80 ± 0.17 mol m^{-2} yr^{-1} and
371 1.07 ± 0.2 mol m^{-2} yr^{-1}, respectively. The annual mean CO_2 flux is improved by 0.27 ± 0.05 mol
372 m^{-2} yr^{-1}.

373 Seasonality in pCO_2 also shows a remarkable improvement during the southwest monsoon
374 period (Figure 6b). The pCO_2 with constZc is considerably lower at a value of 385.22 ± 3.5 µatm
375 during June compared to observational values of 392.83 µatm. However, varZc simulation
376 performs better in terms of pCO_2 variability. The peak value of pCO_2 reaches up to 405.42 ± 5.8
377 µatm. The seasonal mean pCO_2 during the Southwest monsoon period from observations,
378 constZc, and varZc simulations are 397.58 µatm, 389.18 ± 3.6 µatm and 399.95 ± 5.0 µatm,
379 respectively. The improvement in pCO_2 by varZc simulation is 10.76 ± 1.3 µatm when compared
380 with the constZc simulation. This clearly shows that constZc simulation fails to capture the pCO_2
381 driven by upwelling during the Southwest monsoon while the varZc simulation is demonstrably
382 better in representing this seasonal increase. The annual mean pCO_2 from observations, constZc,
383 and varZc simulations are 394.69 µatm, 389.62 ± 3.9 µatm and 391.19 ± 4.7 µatm, respectively.
384 However, it is worth mentioning that there are parts of the year where the constZc performs
385 better compared to varZc. For instance, during MAM as well as in November, the constZc
386 simulation yields a better comparison with the observed pCO_2 whereas varZc simulation yields a
387 reduced magnitude of pCO_2. This may well indicate the biological vs. solubility pump controls
388 on pCO_2 during the intermonsoons. The role of mesoscale variability in the ocean dynamics may
389 also play a role (Valsala and Murtugudde, 2015). Nevertheless, during the most important season

(JJAS) when the pCO_2, CO_2 fluxes, and biological production are found to be dominant in the Arabian Sea, the varZc produces a better simulation.

The improvements shown by the use of varZc in the simulation of CO_2 flux and pCO_2 can be elicited by further analysis of the model biological production. Figure 7 shows the comparison of model export production and new production with observational export production from satellite-derived NPP for constZc and varZc simulations. The model export production in the constZc simulation is much weaker when compared to varZc simulation. The varZc simulation has improved the model export production. Theoretically, the new and export productions in the model should be in balance with each other (Eppley and Peterson, 1979). The constZc export production is much weaker than new production and it is not in balance. In contrast, the varZc simulation yields a close balance among them.

Compared with the observational export production which peaks in August at a value of 154.78 g C m^{-2} yr^{-1}, the varZc simulated export and new productions peak at a value of 160.44 ± 20.4 g C m^{-2} yr^{-1} and 167.18 ± 24.0 g C m^{-2} yr^{-1}, respectively, but in July. A similar peak can be observed in constZc simulated new production as well, with a value of 178.19 ± 28.0 g C m^{-2} yr^{-1}. This apparent shift of one month during JJAS in the model export production as well as in the new production is noted as a caveat in the present set up which will need further investigation. Arabian Sea production is not just limited by nutrients but also the dust inputs (Wiggert et al., 2006). The dust-induced primary production in the WAS, especially over the Oman coast is noted during August (Liao et al., 2016). The mesoscale variability in the circulation and its impact on production and carbon cycle are also a limiting factor in this model as noted above.

411 The seasonal mean export production during the southwest monsoon period from satellite-
412 derived estimate is 123.57 g C m^{-2} yr^{-1}, whereas for constZc and varZc simulations it is 84.81 ±
413 16.0 g C m^{-2} yr^{-1} and 147.19 ± 23.8 g C m^{-2} yr^{-1}, respectively. The new biological
414 parameterization strengthens the model export production by 62.38 ± 7.8 g C m^{-2} yr^{-1} for the
415 southwest monsoon period, which is over a 70% increase. This indicates a considerable impact
416 of the biological pump in the model simulated CO_2 flux and pCO_2 over the WAS. For constZc
417 simulation, the computed new production is slightly higher (150.84 ± 27.9 g C m^{-2} yr^{-1}) than that
418 of varZc (133.03 ± 19.5 g C m^{-2} yr^{-1}). The annual mean export production from observations,
419 constZc and varZc simulations are 94.31 g C m^{-2} yr^{-1}, 77.41 ± 15.1 g C m^{-2} yr^{-1} and 122.54 ± 25.2
420 g C m^{-2} yr^{-1}, respectively.

421 To understand how the varZc parameterization strengthens the export production in the
422 model, we have analyzed the phosphate profiles. It appears that the varZc parameterization
423 allows more phosphate concentration (Figure 8a, b) in the production zone and thereby increases
424 the corresponding biological production (Figure 8c, d). The net export production in the model
425 during JJAS is consistent with the satellite data (Figure 7b). However, in the constZc case, the
426 exports are rather 'flat' throughout the season with a poor representation of seasonal biological
427 export. The Table 1-4 summarize all the values discussed here.

428 The impact of varZc in the biological and solubility pumps is computed as per Louanchi et
429 al., (1996, see Appendix A). The varZc parameterization strengthens the biological as well as the
430 solubility pump in the model thereby modifying the phosphate profiles and achieves a seasonal
431 balance in export versus new production (Figure 9a). During the monsoon period, the varZc
432 simulation increases the strength of the solubility and biological pumps by 10.43 ± 1.3 g C m^{-2}
433 yr^{-1} and 106.52 ± 9 g C m^{-2} yr^{-1}, respectively (see Table 5 and 6). Similarly, the annual mean

strength of solubility pump and the biological pump are increased by 3.29 ± 0.6 g C m^{-2} yr^{-1} and 81.18 ± 9.92 g C m^{-2} yr^{-1}, respectively. This supports the fact that the varZc parameterization basically modifies the biological and solubility pumps in the model simulation and thereby improves the seasonal cycle of CO_2 flux and pCO_2.

3.3 Sri Lanka Dome (SLD)

The seasonal variation in Zc for SLD has a similar pattern as that of WAS. Zc deepens to its maximum during March up to 45.23 ± 0.3 m and reaches its minimum during the following monsoon period at 30.79 ± 1.5 m (Figure 5). The similarities of varZc between WAS and SLD indicates that they both are under similar cycles of solar influx and biological production. The SLD Chl-a dominates only up to July (Vinayachandran et al., 2004) which explains why production with varZc increases earlier compared to WAS which occurs during ASO.

The seasonality in CO_2 flux and pCO_2 were compared with Takahashi et al., (2009) observations (Figure 10). varZc results in a slight improvement in CO_2 flux when compared with constZc (Figure 10a). However, both constZc and varZc simulations underestimate the magnitude of CO_2 flux when compared with observations. The seasonal mean CO_2 flux during the monsoon period is 1.79 mol m^{-2} yr^{-1} from observations, which means SLD region is a source of CO_2. But the mean values of constZc and varZc simulations yield flux values of -0.008 ± 0.2 mol m^{-2} yr^{-1} and 0.24 ± 0.2 mol m^{-2} yr^{-1}, respectively. The constZc simulation misrepresents the SLD region as a sink of CO_2 during monsoon period which is opposite to that of observations. The varZc simulation corrects this misrepresentation to a source albeit at a smaller magnitude by

455 0.24 ± 0.09 mol m^{-2} yr^{-1} for the monsoon period. Compared to observations, the varZc case
456 underestimates the magnitude of JJAS mean by 1.55 mol m^{-2} yr^{-1}.

457 The annual mean CO_2 fluxes for constZc and varZc simulations are -0.02 ± 0.1 mol m^{-2} yr^{-1}
458 and 0.10 ± 0.2 mol m^{-2} yr^{-1}, respectively. The varZc parameterization leads to an improvement of
459 0.13 ± 0.1 mol m^{-2} yr^{-1} in the annual mean CO_2 flux when compared with constZc simulation.
460 The observational annual mean of CO_2 flux is 0.80 mol m^{-2} yr^{-1} which is highly underestimated
461 by both simulations. This indicates a regulation of biological production of the region by varZc
462 which makes this region a source of CO_2 during monsoon. The role of the solubility pump may
463 also be underestimated due to the biases in the physical drivers and the lack of mesoscale eddy
464 activities in these simulations (Prasanna Kumar et al., 2002; Valsala and Murtugudde, 2015).

465 The seasonality of pCO_2 (Figure 10b) especially in the monsoon period is significantly
466 improved. The mean pCO_2 during the monsoon season from observation over the SLD region is
467 382.44 µatm. The seasonal mean pCO_2 during monsoon period for constZc and varZc
468 simulations are 371.67 ± 6.04 µatm and 379.24 ± 8.9 µatm, respectively. The annual mean pCO_2
469 from observations, constZc, and varZc simulations are 380.21 µatm, 370.76 ± 6.1 µatm and
470 374.94 ± 9.6 µatm, respectively. varZc simulations improve the JJAS mean pCO_2 by 7.56 ± 2.8
471 µatm and the annual mean pCO_2 by 4.18 ± 3.5 µatm, which is reflected in CO_2 flux as well. This
472 is likely due to the impact of new biological parameterization in capturing the episodic upwelling
473 in the SLD region which is further investigated by looking at its biological production.

474 The SLD biological production is highly exaggerated by the model for both constZc and
475 varZc simulations (Figure 11a, b). The seasonal mean biological export for the monsoon period
476 is 51.54 g C m^{-2} yr^{-1} as per satellite-derived estimates. However, the constZc and varZc

477 simulations overestimate it at 167.71 ± 59.04 g C m^{-2} yr^{-1} and 151.51 ± 46.4 g C m^{-2} yr^{-1},
478 respectively. This exaggerated export is visible in climatological annual means where for
479 constZc and varZc simulations they are 144.43 ± 49.8 g C m^{-2} yr^{-1} and 156.08 ± 43.8 g C m^{-2} yr^{-1},
480 respectively.

481 For constZc simulation, new production is overestimated from March to October when
482 compared to observations and the second peak is observed in November (Figure 11a). But the
483 overestimate in new production with varZc is observed only during JJAS period by an amount of
484 26.23 g C m^{-2} yr^{-1}. For the SLD region, the varZc parameterization overestimates the export
485 production but minimizes the excess new production, especially in the monsoon period by 64.15
486 ± 36.4 g C m^{-2} yr^{-1}. This indicates that the varZc parameterization is somewhat successful in
487 capturing the upwelling episode during the monsoon over SLD. All values are summarized in
488 Tables 1 to 4.

489 The solubility and biological pumps are modified by the varZc parameterization significantly
490 when compared with the constZc simulation (Figure 9b). Over the monsoon period, the strength
491 of the solubility and biological pumps are improved by 2.81 ± 1.1 g C m^{-2} yr^{-1} and 66.68 ± 9.7 g
492 C m^{-2} yr^{-1}, respectively. Similarly, the annual mean strength of solubility and biological pump
493 are increased by 0.99 ± 1.2 g C m^{-2} yr^{-1} and 52.5 ± 5.1 g C m^{-2} yr^{-1} respectively. All values are
494 provided in Table 5 and 6.

495

496 **3.4 Sumatra Coast (SC)**

497 The seasonal variation in Zc over the SC region lies between 40 m and 46 m (Figure 5). The
498 seasonal maximum occurs during JFM, especially in March with a depth of 45.5 m. During the

499 monsoon period, Zc shoals slightly with a minimum of 41.1 m in July. The variation in Zc is
500 relatively small as compared to the other regions which is consistent with its relatively low
501 production throughout the year.

502 The seasonality of CO_2 flux and pCO_2 captured by constZc and varZc simulations are shown
503 in Figure 12a, b. The varZc simulations overestimate both CO_2 flux and pCO_2, especially during
504 the monsoon. It is found that the constZc simulation is better compared to varZc simulation. The
505 varZc simulation overestimates the seasonal mean CO_2 flux and pCO_2 by 1.19 mol m^{-2} yr^{-1} and
506 29.61 μatm, respectively, compared to observations (Table 1). However, constZc produces a
507 better estimate compared with observations for CO_2 flux and pCO_2. The constZc simulation also
508 delivers a better annual mean than varZc (Table 1, 2). The annual mean bias in constZc and
509 varZc simulations for CO_2 flux is -0.0033 mol m^{-2} yr^{-1} and 0.31 mol m^{-2} yr^{-1}, respectively.
510 Similarly, pCO_2 bias is 1.95 μatm and 9.07 μatm for constZc and varZc simulations.

511 Biological production simulated by the model along SC explains the overestimation of CO_2
512 flux and pCO_2 (Figure 13). Both constZc and varZc simulations greatly overestimate export
513 production in the model. However, a small enhancement in the new production during JJAS in
514 constZc case is an indicator of upwelling episodes. The seasonal mean new production during
515 the monsoon from constZc and varZc are 63.64 ± 30.9 g C m^{-2} yr^{-1} and 78.11 ± 29.1 g C m^{-2} yr^{-1},
516 respectively (Table 4). The seasonal mean export production during the monsoon from
517 observations is 58.87 g C m^{-2} yr^{-1} (Table 3). The constZc simulation represents a better new
518 production, which is seen as a relatively small exaggeration of CO_2 flux and pCO_2. The
519 biological response of SC is found to be better with constZc which is in contradiction to a
520 general improvement found with varZc in the other regions examined here. Such discrepancies
521 over the SC could be due to the effect of Indonesian Throughflow (Bates et al., 2006) which is

not completely resolved in the model due to coarse spatial resolution (also see Valsala and Maksyutov, 2010a).

The overestimation of export production by varZc simulation is also evident by the increase in strength of the biological and solubility pumps, respectively (Figure 9c). The annual mean and JJAS mean DIC increases in the production zone due to the biological pump are 67.21 ± 1.3 g C m^{-2} yr^{-1} and 83.62 ± 0.5 g C m^{-2} yr^{-1}, respectively. Similarly the increase in DIC due to the effect of solubility pump during the JJAS period and annual mean are 10.95 ± 5.2 g C m^{-2} yr^{-1} and 3.87 ± 2.2 g C m^{-2} yr^{-1} respectively (see table 5 and 6).

3.5 Seychelles-Chagos Thermocline Ridge (SCTR)

The SCTR is a unique open-ocean upwelling region with a prominent variability in air-sea interactions (Xie et al., 2002). Wind-driven mixing and upwelling of subsurface nutrient-rich water play a major role in the biological production of this region (Dilmahamod et al., 2016). The seasonal cycle in Zc is shown in Figure 5. The maximum Zc occurs in November at about 44.94 m and the minimum at 33.2 m in July. The shoaling of Zc during the monsoon period shows that the biological parameterization captures the response to upwelling over this region.

The seasonality of CO_2 flux and pCO_2 are shown in Figure 14. The Takahashi observations of CO_2 flux show a peak in June with outgassing of CO_2 during the upwelling episodes. However, both constZc and varZc simulations underestimate this variability. The seasonality of CO_2 flux in varZc shows a significant improvement when compared to constZc simulation, but underestimated when compared to observations. The seasonal mean CO_2 flux during the monsoon from observations, constZc and varZc simulations are 0.82 mol m^{-2} yr^{-1}, -0.32 ± 0.3

544 mol m^{-2} yr^{-1} and -0.05 ± 0.4 mol m^{-2} yr^{-1}, respectively. This represents a reduction in the seasonal
545 mean sink of CO_2 flux in the SCTR region during the monsoon by 0.27 ± 0.1 mol m^{-2} yr^{-1}
546 bringing it closer to a source region (see Table 1 for details).

547 The improved CO_2 flux is also supported by the seasonal cycle in pCO_2. Based on
548 observations, the seasonal mean of pCO_2 with constZc during JJAS is underestimated by 11.47
549 µatm, varZc simulation underestimates it by 6.45 µatm. So it is evident that varZc simulation
550 capture the upwelling episodes better, marked by a larger pCO_2 during JJAS period. However,
551 the magnitude of pCO_2 is still underestimated compared to observations (Table 2).

552 Figure 15 shows the biological production of constZc and varZc simulations for SCTR. It is
553 clear that both simulations overestimate the export production and underestimate the new
554 production. The JJAS mean export production from observations, constZc and varZc are 51.08 g
555 C m^{-2} yr^{-1}, 57.39 ± 14.2 g C m^{-2} yr^{-1} and 99.23 ± 29.8 g C m^{-2} yr^{-1}, respectively. The varZc
556 simulations exaggerate the model export production by 48.14 g C m^{-2} yr^{-1}. The varZc simulation
557 improves the JJAS mean new production by 1.14 ± 2.2 g C m^{-2} yr^{-1} (Table 4). The DIC variations
558 due to the biological pump over the monsoon period and the annual mean also correspond to the
559 exaggerated export production. During the monsoon period, the varZc simulation strengthens the
560 biological and solubility pumps by 72.64 ± 6.2 g C m^{-2} yr^{-1} and -4.56 ± 1.6 g C m^{-2} yr^{-1},
561 respectively, when compared to the constZc simulation (Figure 9d). This is also reflected in the
562 annual mean DIC variations due to the biological and solubility pump effects (see table 5 and 6).
563 This slight improvement in the model new production, especially during the monsoon period
564 signals that the varZc better captures the upwelling over SCTR. Considering the annual mean
565 values of model export and new production, constZc simulation is reasonably faithful to
566 observations.

567 The underestimation of CO_2 and pCO_2, as well as the exaggeration of model export
568 production and a slight, overestimate in model new production may be due to two reasons; (1)
569 SCTR is a strongly coupled region with remote forcing of the mixed layer – thermocline
570 interactions (Zhou et al., 2008) which can affect the seasonality in biological production that the
571 model may not be resolving reasonably, (2) the bias associated with physical drivers, especially
572 wind stress may underestimate the CO_2 flux as well biological production. A similar
573 overestimation of biological production was also reported in a coupled biophysical model
574 (Dilmahamod et al., 2016).

575 Table 1 – 4 shows the entire summary of seasonal and annual mean CO_2 flux, pCO_2 and
576 biological production reported in Section 3.

577

578 **4. Summary and Conclusions**

579 A spatially and temporally varying Zc parameterization as a function of solar radiation and
580 Chl-a is implemented in the biological pump model of OCMIP-II for a detailed analysis of
581 biological fluxes in the upwelling zones of the Indian Ocean. The varZc parameterization
582 improves the seasonality of model CO_2 flux and pCO_2 variability, especially during the monsoon
583 period. A significant improvement is observed in WAS where the monsoon wind-driven
584 upwelling dominates biological production. The magnitude of CO_2 flux matches with
585 observations, especially in July when monsoon winds are at their peak. Monsoon triggers
586 upwelling in SLD as well which acts as a source of CO_2 to the atmosphere. The seasonal and
587 annual mean are underestimated with constZc and the SLD is reduced to a sink of CO_2 flux. The
588 varZc simulation modifies the seasonal and annual means of the CO_2 flux of SLD and depict it as

589 a source of CO_2 especially during the monsoon, but the magnitude is still underestimated
590 compared to Takahashi et al. (2009) observations. The SCTR variability is underestimated by
591 both constZc and varZc simulations, portraying it as a CO_2 sink region whereas observations
592 over the monsoon period indicate that the thermocline ridge driven by the open ocean wind-
593 stress curl is, in fact, an oceanic source of CO_2. However, the varZc simulation reduces the
594 magnitude of the sink in this region bringing it relatively close to observations.

595 VarZc biological parameterization strengthens the export and new productions in the model,
596 which allows it to represent a better seasonal cycle of CO_2 flux and pCO_2 over the study regions.
597 The WAS export production is remarkably improved by 62.37 ± 7.8 g C m^{-2} yr^{-1} compared to
598 constZc. This supports our conclusion that the varZc parameterization increases the strength of
599 biological export in the model. Over the SLD, the JJAS seasonal mean export and new
600 production are underestimated in varZc compared to constZc simulations, but the annual mean
601 export production is improved. Export production at SC and SCTR are highly exaggerated and
602 there is hardly any improvement in new production with a variable Zc especially over the
603 monsoon period. The inability of varZc parameterization to improve the seasonality of SC and
604 SCTR may be due to the interannual variability of biological production associated with the
605 Indonesian throughflow and remote forcing of the mixed layer-thermocline interactions and the
606 effect of biases in the wind stress data used as a physical driver in the model.

607 Sensitivity experiments carried out by prescribing annual mean currents or temperatures over
608 selected subdomains reveal that the varZc retains the seasonality of carbon fluxes, pCO_2, and
609 export and new productions closer to observations. This strongly supports our contention that
610 varZc parameterization improves export and new productions and it is also efficient in capturing
611 upwelling episodes of the study regions. This points out the significant role of having a close

balance in seasonal biological export and new production in models to capture the seasonality in the carbon cycle. This also confirms the role of biological and solubility pumps in producing the seasonality of carbon cycle in the upwelling zones.

However, the underestimation of the seasonality of CO_2 flux over the SLD and overestimation over the SC as well as the SCTR are a cautionary flag for the study. This uncertainty poses an important scientific question as to whether the model biology over the SC and SCTR region is not resolving the seasonality in CO_2 flux and pCO_2 properly or whether the seasonality in the Zc is not able to fully capture the biological processes.

To address these questions we have used an inverse modeling approach (Bayesian inversion) in order to optimize the spatially and temporally varying Zc using surface pCO_2 as the observational constraint and computed the optimized biological production. The results will be reported elsewhere.

Appendix – A

The time evolution equations of the model variables are given by

$$\frac{d[PO_4]}{dt} = L([PO_4]) + J_{PO_4} \qquad (A1)$$

$$\frac{d[DOP]}{dt} = L([DOP]) + J_{DOP} \qquad (A2)$$

$$\frac{dDIC}{dt} = L([DIC]) + J_{DIC} + J_g DIC + J_v DIC \qquad (A3)$$

$$\frac{d[ALK]}{dt} = L([ALK]) + J_{ALK} + J_v ALK \qquad (A4)$$

Where L is the 3D transport operator, which represents the effects of advection, diffusion, and convection. [ ] or square brackets indicate the concentrations in mol m^{-3}. J_{PO_4}, J_{DOP}, J_{DIC}, J_{ALK} are the biological source/sink terms and $J_v DIC$, $J_v ALK$ are the virtual source-sink terms representing the changes in surface DIC and ALK, respectively, due to evaporation and precipitation. $J_g DIC$ is the source-sink term due to air-sea exchange of CO_2.

The following equations represent for the biological processes in the model

For Z < Zc,

$$J_{prod} = \frac{1}{\tau}([PO_4] - [PO_4^*]), \quad [PO_4] > [PO_4^*] \qquad (A5)$$

$$J_{DOP} = \sigma J_{prod} - \kappa[DOP] \qquad (A6)$$

$$J_{PO4} = -J_{prod} + \kappa[DOP] \qquad (A7)$$

$$J_{ca} = Rr_{C:P}(1-\sigma)J_{prod} \quad \text{(A8)}$$

$$J_{DIC} = r_{C:P}J_{PO4} + J_{ca} \quad \text{(A9)}$$

$$J_{ALK} = -r_{N:P}J_{PO4} + 2J_{ca} \quad \text{(A10)}$$

For Z >Zc,

$$J_{prod} = 0, \qquad [PO_4] \leq [PO_4^*] \quad \text{(A11)}$$

$$J_{DOP} = -\kappa[DOP] \quad \text{(A12)}$$

$$J_{PO4} = -\frac{\partial F}{\partial Z} + \kappa[DOP] \quad \text{(A13)}$$

$$F_c = (1-\sigma)\int_0^{Zc} J_{prod}\, dZ \quad \text{(A14)}$$

$$F(Z) = F_c\left(\frac{Z}{Zc}\right)^{-a} \quad \text{(A15)}$$

$$J_{ca} = -\frac{\partial F_{Ca}}{\partial Z} \quad \text{(A16)}$$

$$F_{Ca} = Rr_{C:P}F_C e^{-(Z-Zc)/d} \quad \text{(A17)}$$

Where Z is the depth and Zc is the compensation depth in the model. J_{prod} , J_{Ca} represents the biogeochemical flows with respect to production and calcification. Within Zc, the production of organic phosphorous in the model J_{prod} is calculated using equation A5. $[PO_4]$ is the model phosphate concentration and $[PO_4^*]$ is observational phosphate. τ is the restoration timescale assumed to be 30 days. Whenever the model phosphate exceeds the observational phosphate, it allows production, below which the production is zero. The observational phosphate data were taken from the World Ocean Atlas (WOA; Garcia et al., 2014). It is assumed that a fixed fraction

(σJ_{prod}) of phosphate uptake is converted into Dissolved Organic Phosphorus (DOP) which is a source for J_{DOP} (equation A6). The phosphate not converted to DOP results in an instantaneous downward flux of particulate organic phosphorus at Zc (equation A14). The decrease of flux with depth due to remineralization is shown by a power law relationship as in equation A15. The values of the constants a, κ, σ are 0.9, 0.2/year to 0.7/year, 0.67, respectively. The rate of production is used to explain the formation of calcium carbonate cycle in surface waters (equation A8) and its export is given by equation A16, where R is the rain ratio, a constant molar ratio of exported particulate organic carbon to the exported calcium carbonate flux at Zc. The exponential decrease of calcium carbonate flux with scale depth d is given by equation A17. The biological source or sink of dissolved inorganic carbon (DIC) and alkalinity (ALK) is explained through equations A9 and A10, respectively. Where the values of rain ratio (R) is taken as 0.07 and the Redfield ratio, $r_{C:P} = 117$, and $r_{N:P} = 16$ and scale depth d is chosen as 3500m.

Biological and Solubility Pump calculations

The biological effect on DIC is calculated from Louanchi et al., (1996). The tendency of DIC due to biomass production and calcite formation in the production zone is expressed as below.

$$\left(\frac{\partial DIC}{\partial t}\right)_b = \left(\frac{\partial PO_4}{\partial t}\right)_b \times R_{C:P} - J_{Ca} \qquad \text{(A18)}$$

The total tendency of DIC in the production zone is:

$$\left(\frac{\partial DIC}{\partial t}\right)_{total} = \left(\frac{\partial DIC}{\partial t}\right)_b + \int_x \int_y \mathrm{F} dx\, dy \qquad \text{(A19)}$$

where $\left(\frac{\partial DIC}{\partial t}\right)_b$ is the evolution of DIC due to the impact of biology (i.e., biological pump). The first term in the R.H.S of Equation A18 is the rate of change of phosphate resulting from photosynthesis and respiration in the model (i.e., J_{po4} in this case) multiplied by the carbon to phosphorous Redfield ratio ($R_{C:P}$ = 117:1) and J_{Ca} represents the calcite formation in the model (see Equation A8 & A16). The solubility pump is calculated as the surface integral of the flux F (Louanchi et al., 1996).

Appendix B

In order to compare our model production of organic phosphorous to the curve of Ryther et al., (1956) we have merely scaled our total production to "relative photosynthesis", which is, according to Ryther et al., (1956) an index between 0 and 1 indicating the strength of production estimated as $P_l/P_{max.}$ Here P_l is the photosynthesis at each intensity (of light) of different species and P_{max} is the maximum photosynthesis observed in the same control experiment. The curve between relative photosynthesis and light intensity shows the relation between photosynthetic activity and light in marine phytoplankton. Since our method relates biological production to a function of light (limitation) by Chl-a attenuation, it is the best curve to cross-compare our results. In this case we scaled our total biological production within Zc into relative values between 0-1 by P_l/P_{max}. in which P_l is taken as the individual grid cell biological component of organic phosphorus production and P_{max} is the maximum production available in the domain at any given instant. All the grid points are quite similar to the curve of Ryther et al., (1956) as shown in Figure 2.

Acknowledgements

Thanks to two anonymous reviewers and the editor (Marilaure Grégoire) for comments. Sreeush M. G. sincerely acknowledges the fellowship support from Indian Institute of Tropical Meteorology (IITM) to carry out the study. The OCMIP-II routines were taken from (http://ocmip5.ipsl.jussieu.fr/OCMIP/). GFDL data for OTTM is taken from (http://data1.gfdl.noaa.gov/nomads/forms/assimilation.html). Takahashi data is taken from (http://www.ldeo.columbia.edu/res/pi/CO2/) and SeaWiFS data is obtained from the National Aeronautics and Space Administration (NASA) Ocean Color Website (http://oceancolor.gsfc.nasa.gov/). The computations were carried out in High-Performance Computing (HPC) facility of Ministry of Earth Sciences (MoES), IITM.

References

Anderson, L. A., Sarmiento, J. L.: Global ocean phosphate and oxygen simulations, Global Biogeochem. Cycles, 9, 621-636, doi:10.1029/95GB01902, 1995.

Asselin, R.: Frequency filter for time integrations, Mon. Wea. Rev., 100, 487–490, doi: 10.1175/1520-0493, 1972.

Banse, K., McClain, C. R.: Winter blooms of phytoplankton in the Arabian Sea as observed by the Coastal Zone Color Scanner, Mar. Ecol. Prog. Ser, 34, 201 – 211, 1986.

Banse, K.: Seasonality of phytoplankton chlorophyll in the central and northern Arabian Sea, Deep Sea Res., 34, 713 – 723, doi:10.1016/0198-0149, 1987.

Barber, R. T., Marra. J., Bidigare. R. C., Codispoti. L. A., Halpern. D., Johnson. Z., Latasa. M., Goericke. R., and Smith. S. L.: Primary productivity and its regulation in the Arabian Sea during 1995, Deep. Sea. Res. pt. II, 48, 1127 – 1172. doi:10.1016/S0967-0645, 2001.

Bates, N. R., Pequignet. A. C., and Sabine. C. L.: Ocean carbon cycling in the Indian Ocean: 2. Estimates of net community production, Global Biogeochem. Cycles., 20, GB3021, doi:10.1029/2005GB002492, 2006.

Bauer, S., Hitchcock, G. L., Olson, D. B.: Influence of monsoonally-forced Ekman dynamics upon surface-layer depth and plankton biomass distribution in the Arabian Sea, Deep Sea Res., 38, 531 – 553, doi:10.1016/0198-0149, 1991.

Behrenfeld, M. J., Falkowski. P. G.: Photosynthetic rates derived from satellite-based chlorophyll concentration, Limnol. Oceanogr., 42, 1 – 20, doi: 10.4319/lo.1997.42.1.0001, 1997.

742 Boyd, P. W., Rynearson, T. A., Armstrong, E. A., Fu. F., Hayashi. K. and co-authors.: Marine
743 Phytoplankton Temperature versus growth responses from polar to tropical waters – outcome of
744 a scientific community-wide study, PLoS ONE 8(5)., e63091,
745 Doi:10.1371/journal.phone.0063091, 2013.

746 Brock, J C., McClain, C. R.: Interannual variability of the southwest monsoon phytoplankton
747 bloom in the north-western Arabian Sea, J. Geophys. Res., 97(C1), 733 – 750,
748 doi/10.1029/91JC02225, 1992a.

749 Brock, J. C., McClain, C. R., Hay, W. W.: A southwest monsoon hydrographic climatology for
750 the northwestern Arabian Sea, J. geophys. Res., 97(C6), 9455 – 9465, doi: 10.1029/92JC00813,
751 1992b.

752 Brock, J. C., McClain, C. R., Luther, M. E., Hay, W. W.: The phytoplankton bloom in the
753 northwestern Arabian Sea during the southwest monsoon of 1979, J. Geophys. Res., 96(C11),
754 623 – 642, doi: 10.1029/91JC01711, 1991.

755 Brock. J., Sathyendranath. S., and Platt. T.: Modelling the seasonality of subsurface light and
756 primary production in the Arabian Sea, Mar. Eco. Prog. Ser., 101, 209 – 221, 1993.

757 Bruce, J. G.: Some details of upwelling off the Somali and Arabian coasts, J. Mar. Res., 32, 419
758 – 423, 1974.

759 Bryan. K., Lewis, L. J.: A water mass model of the world ocean, J. Geophys. Res., 84, 2503 –
760 2517, doi: 10.1029/JC084iC05p02503, 1979.

761 Chang, Y. S., Zhang. S., Rosati. A., Delworth. T., Stern. W. F.: An assessment of oceanic
762 variability for 1960-2010 from the GFDL ensemble coupled data assimilation, Clim. Dyn., 40,
763 775 – 803, doi: 10.1007/s00382-012-1412-2, 2012.

764 Christian J. R., Verschall M. A., Murtugudde R., Busalacchi A. J., McClain C. R.:
765 Biogeochemical modeling of the tropical Pacific Ocean. II: Iron biogeochemistry, Deep Sea
766 Res., 49, 545 – 565, doi:10.1016/S0967-0645, 2001.

767 Colwell, R. R.: Global climate and infectious disease: the cholera paradigm, Science., 274(5295),
768 2025 – 2031, doi: 10.1126/science.274.5295.2025, 1996.

769 Dickson, A. G., and F. J. Millero.: A comparison of the equilibrium constants for the dissociation
770 of carbonic acid in seawater media, Deep-Sea Res., 34, 1733 – 1743, 1987.

771 Dilmahamod A. F., Hermes. J. C., Reason C. J. C.: Chlorophyll-a variability in the Seychelles-
772 Chagos Thermocline Ridge: Analysis of a coupled biophysical model, J. of. Mar. Sys., 154, 220
773 – 232, doi:10.1016/j.jmarsys.2015.10.011, 2016.

774 Doney S. C., and co-authors.: Evaluating global ocean carbon models: The importance of
775 realistic physics, Glob. Biogeochem. Cycles, 18, doi:10.1029/2003GB002150, 2004.

776 Eppley, R. W., Peterson. B. J.: Particulate organic matter flux and planktonic new production in
777 the deep ocean, Nature, 282, 677-680, doi:10.1038/282677a0, 1979.

778 Eppley, R. W.: Temperature and phytoplankton growth in the sea, Fish. Bull., 70, 1063 – 1085,
779 1972.

780 Falkowski, P. G., E. A. Laws, R. T. Barber, and J. W. Murray: phytoplankton and their role in
781 the primary, new and export production, In: Fasham M.J.R (eds) Ocean Biogeochemistry, Global

782 Change – The IGBP series (closed). Springer, Berlin, Heidelberg, doi:
783 https://doi.org/10.1007/978-3-642-55844-3_5, 2003.

784 Feely, R. A., Sabine, C. L., Takahashi, T., Wanninkhof, R.: Uptake and Storage of Carbon
785 Dioxide in the Ocean: The Global CO_2 Survey, Oceanography., 14(4), 18–32,
786 doi:10.5670/oceanog.2001.03, 2001.

787 Friedrichs, M. A. M., and co-authors.: Assessment of skill and portability in regional
788 biogeochemical models: role of multiple planktonic groups, J. Geophy. Res., 112, doi:
789 10.1029/2006JC003852, 2007.

790 Friedrichs, M. A. M., Hood, R. R., Wiggert, J. D.: Ecosystem complexity versus physical forcing
791 quantification of their relative impact with assimilated Arabian Sea data, Deep Sea Res., 53, 576-
792 600, doi:10.1016/j.dsr2.2006.01.026, 2006.

793 Garcia, H. E., R. A. Locarnini, T. P. Boyer, J. I. Antonov, O.K. Baranova, M.M. Zweng, J.R.
794 Reagan, D.R. Johnson.: World Ocean Atlas 2013, Volume 4: Dissolved Inorganic Nutrients
795 (phosphate, nitrate, silicate), S. Levitus, Ed., A. Mishonov Technical Ed.; NOAA Atlas NESDIS
796 76, 25 pp, 2014.

797 Gattuso, J. P., B. Gentili, C. M. Duarte, J. A. Kleypas, J. J. Middelburg, and D. Antoine.: Light
798 availability in the coastal ocean: Impact on the distribution of benthic photosynthetic organisms
799 and their contribution to primary production, Biogeosciences, 3, 489 – 513, doi:10.5194/bg-3-
800 489-2006, 2006.

801 Gent, P. R., McWilliams. J. C.: Isopycnal mixing in ocean circulation models, J. Phys.
802 Oceanogr., 20, 150 – 155, doi: 10.1175/15200485, 1990.

803 Harwell, C., Kim, K., Burkholder, J., Colwell, R., Epstein, P. R., Grimes, D., Hofmann, E. E.,
804 Lipp, E. K., Osterhaus, A., and Overshreet, R. M.: Emerging marine diseases-climate links and
805 anthropogenic factors, Science., 285(5433), 1505 – 1510, doi: 10.1126/science.285.5433.1505,
806 1999.

807 Jerlov N. G.: Marine optics, Second ed., Elsevier, pp 231, 1976.

808 Jung, E., and Kirtman. B. P.: ENSO modulation of tropical Indian ocean subseasonal variability,
809 Geophys. Res. Lett., 43, doi: 10.1002/2016GL071899, 2016.

810 Keeling, C. D., Whorf, T. P., Wahlen, M., and van der plicht, J.: Interannual extremes in the rate
811 of rise of atmospheric carbon dioxide since 1980, Nature, 375, 666 – 670, 1995.

812 Key, R. M., et al,.: A global ocean carbon climatology: Results from Global Data Analysis
813 Project (GLODAP), Global Biogeochem. Cycles, 18, GB4031, doi:10.1029/2004GB002247,
814 2004

815 Krey, J., Bahenerd, B.: Phytoplankton production atlas of the international Indian Ocean
816 expedition, Institut fur Meereskundeander Universitat Kiel, Kiel, German, 1976.

817 Large, W. G., McWilliams, J. C., Doney, S. C.: Oceanic vertical mixing: A review and a model
818 with a nonlocal boundary layer parameterization, Rev. Geophys., 32, 363 – 403, doi:
819 10.1029/94RG01872, 1994.

820 Laws, E. A., P. G. Falkowski, W.O. Smith, Jr., H. Ducklow and J. J. McCarthy: Temperature
821 effects on export production in the open ocean, Global Biogeochem. Cycles, 14, 1231 – 1246,
822 2000.

Le Quere, C., Orr, J. C., Monfray, P., Aumont, O.: Interannual variability of the oceanic sink of CO_2 from 1979 through 1997, Global Biogeochem. Cycles., 14, p1247 – 1265, doi: 10.1029/1999GB900049, 2000.

Lee, P. F., Chen, I. C., Tzeng. W. N.: Spatial and Temporal distributions patterns of bigeye tuna (Thunnusobsesus) in the Indian Ocean, Zoological studies-Taipei-, 44(2), 260, 2005.

Lehodey .P., Senina I., Sibert. J., Bopp. L., Calmettes B., Hampton .J., Murtugudde. R.: Preliminary forecasts of Pacific bigeye tuna population trends under the A2 IPCC scenario, Prog in Oceanography., 86, 302 – 315, doi:10.1016/j.pocean.2010.04.021, 2010.

Liao, X., Zhan, H., Du, Y.: Potential new production in two upwelling regions of the Western Arabian Sea: Estimation and comparison, J. Geophys. Res. Oceans., 121, doi:10.1002/2016JC011707, 2016.

Lopez-Urrutia, A., E. San Martin, R. P. Harris, and X. Irigoien.: Scaling the metabolic balance of the oceans, Proc. Natl. Acad. Sci. U.S.A., 103, 8739-8744,doi:10.1073/pnas.0601137103, 2006.

Louanchi. F., N. Metzl., and Alain Poisson.: Modelling the monthly sea surface f_{CO2} fields in the Indian Ocean, Marine Chemistry, 55, 265 – 279, 1996.

Marra, J. F., Veronica P. Lance, Robert D. Vaillancourt, Bruce R. Hargreaves.: Resolving the ocean's euphotic zone, Deep Sea. Res. pt. I., 83, 45 -50, doi:10.1016/j.dsr.2013.09.005, 2014.

Matsumoto K., Tokos. K. S., Price., A. R., Cox. S. J.: First description of the Minnesota Earth System Model for Ocean biogeochemistry (MESMO 1.0), Geosci. Model Dev., 1, 1-15, doi:10.5194/gmd-1-1-2008, 2008.

McCreary, J., Murtugude, R., Vialard, J., Vinayachandran, P., Wiggert, J. D., Hood, R. R., Shankar, D., Shetye, S.: Biophysical processes in the Indian Ocean, Indian Ocean Biogeochemical Processes and Ecological Variability., 9 – 32, doi: 10.1029/GM185, 2009.

Mehrbach, C., C. H. Culberson, J. E. Hawley, and R. M. Pytkowicz.: Measurement of the apparent dissociation constants of carbonic acid in seawater at atmospheric pressure, Limnol. Oceanogr., 18, 897 – 907, 1973.

Moisan, J. R., Moisan, A. T., Abbott, M. R.: Modelling the effect of temperature on the maximum growth rates of phytoplankton populations, Eco. Modelling., 153, 197-215, doi:10.1016/S0304-3800(02)00008, 2002.

Morel, A.: Optical modeling of the upper ocean in relation to its biogenous matter content (Case 1 Waters), J. Geophys. Res., 93, 10479-10, 768, doi: 10.1029/JC093iC09p10749, 1988.

Murtugudde R., McCreary J. P., Busalacchi, A. J.: Oceanic processes associated with anomalous events in the Indian Ocean with relevance to 1997-1998, J. Geophys. Res., 105, 3295-3306, doi: 10.1029/1999JC900294, 2000.

Murtugudde, R. G., S. R. Signorini, J. R. Christian, A. J. Busalacchi, C. R. McClain, and J. Picaut.: Ocean color variability of the tropical Indo-Pacific basin observed by SeaWiFS during 1997 – 1998, J. Geophys. Res., 104(C8), 18351 – 18366, doi.10.1029/1999JC900135, 1999a.

Murtugudde, R., Busalacchi, A. J.: Interannual variability of the dynamics and thermodynamics of the tropical Indian Ocean, J. Clim. 12, 2300-2326, doi:10.1175/1520-0442, 1999b.

Murtugudde, R., Seager, R., Thoppil, P.: Arabian Sea response to monsoon variations, Paleoceanography., 22, PA4217, doi:10.1029/2007PA001467, 2007.

Najjar, R. G., Keeling, R. F.: Analysis of the mean annual cycle of the dissolved oxygen anomaly in the world ocean, J. Mar. Res., 55, 117 – 151, doi:10.1357/0022240973224481, 1997.

Najjar, R. G., Orr, J. C.: Design of OCMIP-2 simulations of chlorofluorocarbons, the solubility pump and common biogeochemistry, http://www.ipsl.jussieu.fr/OCMIP/., 1998.

Najjar, R. G., Sarmiento, J. L., Toggweiler, J. R.: Downward transport and fate of organic matter in the ocean: simulations with a general circulation model, Global Biogeochem. Cycles., 6, 45-76, doi/10.1029/91GB02718, 1992.

Naqvi, S. W. A., Moffett, J. W., Gauns, M. U., Narvekar, P. V., Pratihary, A. K., Naik, H., Shenoy, D. M., Jayakumar, D. A., Goepfert, T. J., Patra, P. K., Al-Azri, A., and Ahmed, S. I.: The Arabian Sea as a high-nutrient, low-chlorophyll region during the late Southwest Monsoon, Biogeosciences., 7, 2091-2100, doi:10.5194/bg-7-2091-2010, 2010.

Naqvi, S., Naik, H., Narvekar, P.: The Arabian Sea, in Biogeochemistry, edited by K. Black and G. Shimmield, pp. 156 – 206, Blackwell, Oxford, 2003.

Orr, J. C., and co-authors.: Anthropogenic ocean acidification over the twenty-first century and its impact on calcifying organisms, Nature, 437, 681 – 686, doi:10.1038/nature04095, 2005.

Orr, J. C., and co-authors.: Estimates of anthropogenic carbon uptake from four three-dimensional global ocean models, Glob. Biogeochem. Cycles., 15, p43 – 60, doi: 10.1029/2000GB001273, 2001.

Orr, J. C., Aumont, O., Bopp, L., Calderia, K., Taylor, K., et. al.: Evaluation of seasonal air-sea CO2 fluxes in the global carbon cycle models, International open Science conference (Paris, 7-10 Jan. 2003), 2003.

885 Osawa, T., Julimantoro, S.: Study of fishery ground around Indonesia archipelago using remote
886 sensing data, International archives of the Photogrammetry, Remote sensing and spatial
887 information science., vol XXXVIII, part-8, 2010.

888 Parsons, T. R., Takahashi, M., Habgrave, B.: In Biological Oceanographic Processes, 3rd ed.,
889 330pp., Pergamon Press, New York, doi: 10.1002/iroh.19890740411, 1984.

890 Prasanna Kumar, .S., Muraleedharan, P. M., Prasad, T. G., Gauns, M., Ramaiah, N., de Souza, S.
891 N., Sardesai, S., Madhupratap, M.: Why is the Bay of Bengal less productive during summer
892 monsoon compared to the Arabian Sea?, Geophys. Res. Lett., 29(24), 2235,
893 doi:10.1029/2002GL016013, 2002.

894 Prasanna Kumar, S., Roshin, P. R., Narvekar, J., Dinesh Kumar, P., Vivekanandan, E.: What
895 drives the increased phytoplankton biomass in the Arabian Sea?, Current Science, 99(I), 101 –
896 106, 2010.

897 Prassana Kumar. S, Ramaiah. N, Gauns. M., Sarma V. V. S. S., Muraleedharan. P. M.,
898 RaghuKumar. S., Dileep Kumar., Madhupratap. M.: Physical forcing of biological productivity
899 in the Northern Arabian Sea during the Northeast Monsoon, Deep Sea Res. Pt. II., 48, 1115-
900 1126, doi:10.1016/S0967-0645(00)00133-8, 2001.

901 Praveen, V., Ajayamohan**,** R. S., **Valsala,** V., Sandeep, S.: Intensification of upwelling along
902 Oman coast in a warming scenario, Geophys. Res. Lett., 43, doi:10.1002/2016GL069638, 2016.

903 Press, W. H., and others: Numerical Recipes in FORTRAN. Cambridge University Press,
904 Cambridge, England, 1996.

905 Qasim, S. Z.: Biological productivity of the Indian Ocean, J. Mar. Sci., 6, 122 – 137, 1977.

906 Qasim, S. Z.: Oceanography of Northern Arabian Sea, Deep Sea Res., 29(9A), 1041 – 1068,
907 doi:10.1016/0198-0149(82)90027-9, 1982.

908 Redi, M.: Oceanic isopycnal mixing by coordinate rotation, J. Phys. Oceanogr., 12, 1154 – 1158,
909 doi: 10.1175/1520-0485, 1982.

910 Regaudie-de-Gioux, A., and C. M. Duarte.: Compensation irradiance for planktonic community
911 metabolism in the ocean, Global Biogeochem. Cycles, 24, GB4013,
912 doi:10.1029/2009GB003639, 2010.

913 Roxy, M. K., Modi, A., Murtugudde, R., Valsala, V., Panickal, S., Prasanna Kumar, S.,
914 Ravichandran, M., Vichi, M., Levy, M.: A reduction in marine primary productivity driven by
915 rapid warming over the tropical Indian Ocean, 43, 826 – 833, J. Geophys. Res. Letters.,
916 doi:10.1002/2015GL066979, 2015.

917 Ryther, J., Menzel, D.: On the production, composition, and distribution of organic matter in the
918 Western Arabian Sea, Deep Sea Research and Oceanographic Abstracts., 12(2), 199 -209.
919 doi:10.1016/0011-7471(65)90025-2, 1965.

920 Ryther, J.: Photosynthesis in the ocean as function of light Intensity, Limnol. Oceanogr., vol 1,
921 issue 1, doi: 10.4319/lo.1956.1.1.0061, 1956.

922 Sarma V. V. S. S.: Net plankton community production in the Arabian Sea based on O_2 mass
923 balance model, Glob. Biogeochem. Cycles., 18, GB4001, doi:10.1029/2003GB002198, 2004.

924 Sarma, V. V. S. S.: An evaluation of physical and biogeochemical processes regulating the
925 perennial suboxic conditions in the water column of the Arabian Sea, Global Biogeochem.
926 Cycles., 16, doi:10.1029/2001GB001461, 2002.

927 Sarmiento, J. L., and Gruber, N.: Ocean Biogeochemical Dynamics, Princeton University Press,
928 New Jersey, 2006.

929 Sarmiento, J. L., Monfray. P., Maier-Reimer., Aumont, O., Murnane, R. J., Orr, J. C.: Sea-air
930 CO_2 fluxes and carbon transport: A comparison of three ocean general circulation models,
931 Global Biogeochem. Cycles., 14, p1267 – 1281. doi: 10.1029/1999GB900062, 2000.

932 Schott, F.: Monsoon response of the Somali current and associated upwelling, Prog.Oceanogr.,
933 12, 357 – 381, doi:10.1016/0079-6611(83)90014-9, 1983.

934 Smetacek, V., and Passow, U.: Spring bloom initiation and Sverdrup's critical depth model,
935 Limnol. Oceanogr., 35, 228 – 234, doi: 10.4319/lo.1990.35.1.0228, 1990.

936 Smith, L. S.: Understanding the Arabian Sea: Reflections on the 1994-1996 Arabian Sea
937 Expedition, Deep Sea Res. Pt. II., 48, 1385-1402, doi:10.1016/S0967-0645(00)00144-2, 2001.

938 Smith, R. L., Bottero, L. S.: On upwelling in the Arabian Sea. In Angel, M (ed) A voyage of
939 Discovery. Pergamon Press, New York, p. 291 – 304, 1977.

940 Smith, S. L., Codispoti, L. A.: Southwest monsoon of 1979: chemical and biological response of
941 Somali coastal waters. Science, 209, 597 – 600. doi:10.1126/science.209.4456.597, 1980.

942 Smith, S. L.: Biological indications of active upwelling in the northwestern Indian Ocean in 1964
943 and 1979, a comparison with Peru and northwest Africa, Deep Sea Res., 31, 951 – 967,
944 doi:10.1016/0198-0149(84)90050-5, 1984.

945 Susanto. R., Gordon, A. L., Zheng. Q.: Upwelling along the coasts of Java and Sumatra and its
946 relation to ENSO, J. Geophys. Res. Lett., 28, 1599-1602, doi: 10.1029/2000GL011844, 2001.

947 Swallow, J. C.: Some aspects of the physical oceanography of the Indian Ocean, Deep Sea Res.,
948 31, 639 – 650, doi:10.1016/0198-0149(84)90032-3, 1984.

949 Takahashi, T., Sutherland, S. C., Wanninkhof, R., Sweeney, C., Feely, R. A., Chipman, D. W.,
950 Hales, B., Friederich, G., Chavez, F., Sabine, C., et al.: Climatological mean and decadal
951 changes in surface ocean pCO_2 and net sea-air CO_2 flux over the global oceans. Deep Sea Res.,
952 Pt. II., 56, 554 – 557, doi:10.1016/j.dsr2.2008.12.009, 2009.

953 Valsala V., Maksyutov, S.: A short surface pathway of the subsurface Indonesian Throughflow
954 water from the Java Coast associated with upwelling, Ekman Transport, and Subduction. Int. J.
955 Oceanogr., 15, doi: 10.1155/2010/540743, 2010a.

956 Valsala V., Maksyutov, S.: Interannual variability of air-sea CO_2 flux in the north Indian Ocean,
957 Ocean Dynamics., 1 – 14, doi 10.1007/s10236-012-0588-7, 2013.

958 Valsala V., R. R. Rao.: Coastal Kelvin waves and dynamics of gulf of Aden eddies, Deep Sea
959 Res., Pt. I., 116, 174 – 186, https://doi.org/10.1016/j.dsr.2016.08.003, 2016.

960 Valsala, K. V., Maksyutov, S., Ikeda, M.: Design and Validation of an offline oceanic tracer
961 transport model for a carbon cycle study, J. clim., 21, doi: 10.1175/2007JCLI2018.1, 2008.

962 Valsala, V**.,** Maksyutov, S., Murtugudde, R.: Interannual to Interdecadal Variabilities of the
963 Indonesian Throughflow Source Water Pathways in the Pacific Ocean, J. Phys. Oceanogr., 41,
964 1921–1940, doi: 10.1175/2011JPO4561.1, 2011.

965 Valsala, V., Maksyutov, S.: Simulation and assimilation of global **oc**ean pCO_2 and air-sea CO_2
966 fluxes using ship observations of surface ocean pCO_2 in a simplified biogeochemical model,
967 Tellus., 62B, doi: 10.1111/j.1600-0889.2010.00495, 2010b.

968 Valsala, V., Murtugudde, R.: Mesoscale and Intraseasonal Air-Sea CO_2 Exchanges in the
969 Western Arabian Sea during Boreal Summer, Deep Sea Res. Pt. I, 103, 103-113,
970 doi:10.1016/j.dsr.2015.06.001, 2015.

971 Valsala, V., Roxy, M., Ashok, K., Murtugudde, R.: Spatio-temporal characteristics of seasonal to
972 multidecadal variability of pCO_2 and air-sea CO_2 fluxes in the equatorial Pacific Ocean, J.
973 Geophys. Res., 119, 8987 – 9012, doi:10.1002/2014JC010212, 2014.

974 Valsala, V.: Different spreading of Somali and Arabian coastal upwelled waters in the northern
975 Indian Ocean: A case study. J. Phy. Oceanogr., 803 – 816, doi: https://doi.org/10.1007/s10872-
976 009-0067-z, 2009.

977 Vialard, J. and co-authors.: Air-Sea Interactions in the Seychelles-Chagos Thermocline Ridge
978 Region, BAMS, doi:10.1175/2008BAMS2499.1, 2009.

979 Vinayachandran P. N., Yamagata, T.: Monsoon Response of the Sea around Sri Lanka:
980 Generation of Thermal Domes and Anticyclonic Vortices, J. Phy. Oceano., 28, 1946 – 1960, doi:
981 10.1175/1520-0485, 1998.

982 Vinayachandran, P. N., Chauhan, P., Mohan, M., Nayak, S.: Biological response of the sea
983 around Sri Lanka to summer monsoon, Geophys. Res. Lett., 31, L0I302,
984 doi:10.1029/2003GL018533, 2004.

985 Wang .X. J., Behrenfeld. M., Le Borgne .R., Murtugudde .R., and Boss. E.: Regulation of
986 phytoplankton carbon to chlorophyll ratio by light, nutrients and temperature in the equatorial
987 Pacific Ocean: a basin-scale model. Biogeosciences., 6, 391 – 404, doi:10.5194/bg-6-391-2009,
988 2009.

989 Weiss, R. F.: Carbon dioxide in water and seawater: The solubility of a non-ideal gas, Mar.
990 Chem., 2, 203-215, 1974.

991 Wiggert J. D., Jones. B. H., Dickey .T D., Brink .K. H., Weller .R .A., Marra. J., Codispoti. L.
992 A.: The Northeast Monsoon's impact on mixing, phytoplankton biomass and nutrient cycling in
993 the Arabian Sea, Deep Sea Res. Pt. II, 47, 1353-1385, doi:10.1016/S0967-0645(99)00147-2,
994 2000.

995 Wiggert, J. D., Hood, R. R., Banse, K., Kindle, J. C.: Monsoon-driven biogeochemical processes
996 in the Arabian Sea, Progr. Oceanogr., 65, 176-213, doi:10.1016/j.pocean.2005.03.008, 2005.

997 Wiggert. J. D., Murtugudde, R. G., Christian J. R.: Annual ecosystem variability in the tropical
998 Indian Ocean: results of a coupled bio-physical ocean general circulation model, Deep Sea Res.
999 Pt. II., 53, 644-676, doi:10.1016/j.dsr2.2006.01.027, 2006.

1000 Xie, S. P., Annamalai, H., Schott, F. A., McCreary Jr. J. P.: Structure and mechanism of south
1001 Indian ocean climate variability, J. clim., 15, 864 – 878, doi: 10.1175/1520-0442, 2002.

1002 Xing W., Xiaomei. L., Haigang Z., Hailong. L.: Estimates of potential new production in the
1003 Java-Sumatra upwelling system, Chinese Journal of Oceanology and Limnology., 30, 1063-
1004 1067, doi:10.1007/s00343-012-1281, 2012.

1005 Yamanaka, Y., Yoshie, N, Masahiko Fujii, Maka .N. Aita and Kishi. M. J.: An Ecosystem
1006 coupled with Nitrogen-Silicon-Carbon cycles applied to station A7 in the Northwestern Pacific,
1007 J. of Oceanogr., 60, p227-241, doi: 10.1023/B:JOCE.0000038329.91976.7d, 2004.

1008 Zhou X., Weng. E., Luo., Y.: Modelling patterns of nonlinearity in the ecosystem responses to
1009 temperature, CO_2 and precipitation changes, Eco. Appli., 18, 453 – 466, doi: 10.1890/07-0626.1,
1010 2008.

1011

Table: 1 WAS = Western Arabian Sea, SLD = Sri Lanka Dome, SC = Sumatra Coast, SCTR = Seychelles-Chagos Thermocline Ridge. JJAS mean and the climatological annual mean of CO_2 flux from Takahashi observations, constZc, and varZc simulations. Units are mol m^{-2} yr^{-1}.

Regions	CO_2 flux (mol m^{-2} yr^{-1})					
	JJAS Mean			Annual Mean		
	OBS	constZc	varZc	OBS	constZc	varZc
WAS	1.99	1.44 ± 0.2	2.31 ± 0.4	0.94	0.80 ± 0.1	1.07 ± 0.2
SLD	1.79	-0.008 ± 0.2	0.24 ± 0.09	0.8	-0.02 ± 0.1	0.10 ± 0.2
SC	0.31	0.60 ± 0.5	1.51 ± 1.01	0.21	0.21 ± 0.3	0.53 ± 0.5
SCTR	0.82	-0.32 ± 0.3	-0.05 ± 0.4	0.55	-0.02 ± 0.1	-0.07 ± 0.2

Table: 2 Same as Table 1, but for pCO_2. Units are µatm.

Regions	pCO_2 (µatm)					
	JJAS Mean			Annual Mean		
	OBS	constZc	varZc	OBS	constZc	varZc
WAS	397.58	389.18 ± 3.7	399.95 ± 5.01	394.69	389.62 ± 3.9	391.19 ± 4.7
SLD	382.44	371.67 ± 6.04	379.24 ± 8.9	380.21	370.76 ± 6.1	374.94 ± 9.6
SC	372.52	382.36 ± 12.7	402.14 ± 21.8	372.69	374.65 ± 9.3	381.76 ± 13.6
SCTR	377.18	365.71 ± 5.08	370.72 ± 7.4	379.89	372.69 ± 4.7	369.00 ± 5.4

Table: 3 JJAS mean and the climatological annual mean of export production from satellite-derived Net Primary Production data, constZc, and varZc simulations. Units are g C m^{-2} yr^{-1}.

Regions	Export Production (g C m^{-2} yr^{-1})					
	JJAS Mean			Annual Mean		
	OBS	constZc	varZc	OBS	constZc	varZc
WAS	123.57	84.81 ± 16.04	147.19 ± 23.8	94.31	77.41 ± 15.1	122.54 ± 25.2
SLD	51.54	167.71 ± 59.04	151.51 ± 46.4	43.25	144.43 ± 49.8	156.08 ± 43.8
SC	58.87	260.11 ± 104.7	310.03 ± 99.5	54.53	172.52 ± 72.4	215.52 ± 70.8
SCTR	51.08	57.39 ± 14.2	99.23 ± 21.8	40.45	55.15 ± 17.9	80.35 ± 26.04

Table: 4 Model derived values for New production. Units are g C m^{-2} yr^{-1}.

Regions	New Production (g C m^{-2} yr^{-1})					
	JJAS Mean			Annual Mean		
	OBS	constZc	varZc	OBS	constZc	varZc
WAS	--	150.84 ± 27.9	133.03 ± 19.5	--	108.43 ± 23.4	81.47 ± 15.7
SLD	--	141.93 ± 64.1	77.78 ± 27.6	--	111.05 ± 71.1	50.37 ± 26.3
SC	--	63.64 ± 30.9	78.11 ± 29.1	--	56.69 ± 43.3	54.58 ± 23.3
SCTR	--	12.17 ± 16.3	13.32 ± 18.6	--	13.74 ± 15.5	12.94 ± 13

Table 5: Biological pump impact over DIC in the model due to constZc and varZc simulations for JJAS and annual mean.

Regions	Biological Pump (g C m^{-2} yr^{-1})			
	constZc		varZc	
	JJAS Mean	Annual Mean	JJAS Mean	Annual Mean
WAS	45.18 ± 14.8	45.49 ± 14.38	151.7 ± 23.8	126.67 ± 24.3
SLD	89.39 ± 58.1	108.65 ± 48.6	156.07 ± 48.4	161.15 ± 43.5
SC	235.54 ± 95.4	155.21 ± 67.4	319.16 ± 94.9	222.92 ± 68.7
SCTR	30.49 ± 13.4	26.81 ± 16.8	103.13 ± 19.6	83.98 ± 23.6

Table 6: Same as Table 5, But for Solubility pump.

Regions	Solubility Pump (g C m^{-2} yr^{-1})			
	constZc		varZc	
	JJAS Mean	Annual Mean	JJAS Mean	Annual Mean
WAS	17.29 ± 3.5	9.63 ± 2.1	27.72 ± 4.8	12.92 ± 2.7
SLD	-0.09 ± 2.4	-0.32 ± 2.3	2.9 ± 3.5	1.31 ± 3.5
SC	7.22 ± 6.9	2.56 ± 3.8	18.17 ± 12.1	6.43 ± 6.0
SCTR	-3.95 ± 3.7	-0.35 ± 2.3	-0.61 ± 5.3	-0.86 ± 2.8

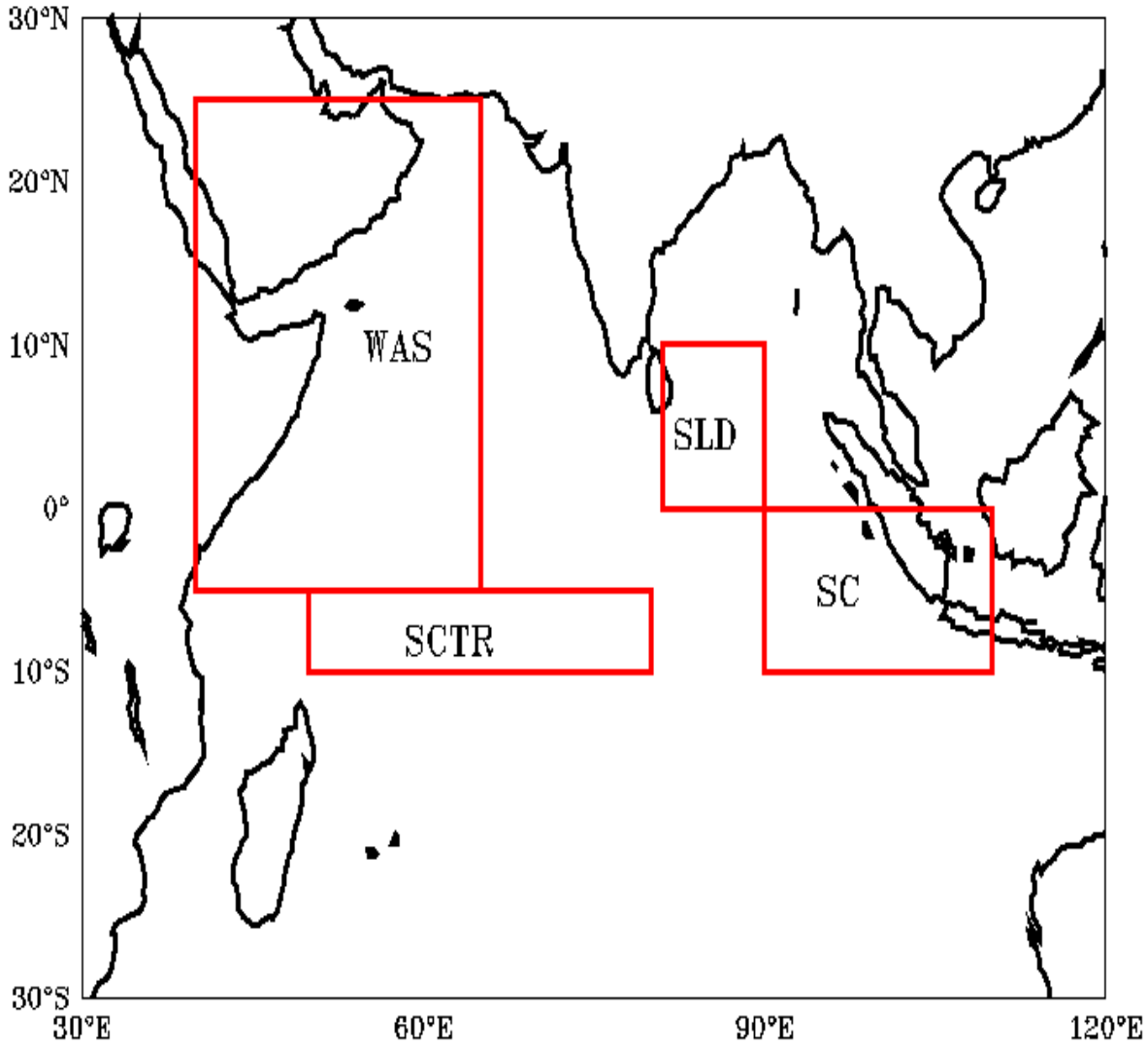

Figure 1: Red boxes shows the study regions (1) WAS (Western Arabian Sea, 40°E:65°E, 5°S:25°N) (2) SLD (Sri Lanka Dome, 81°E:90°E, 0°:10°N) (3) SCTR (Seychelles-Chagos Thermocline Ridge, 50°E:80°E, 5°S:10°S) and (4) SC (Sumatra Coast, 90°E:110°E, 0°:10°S).

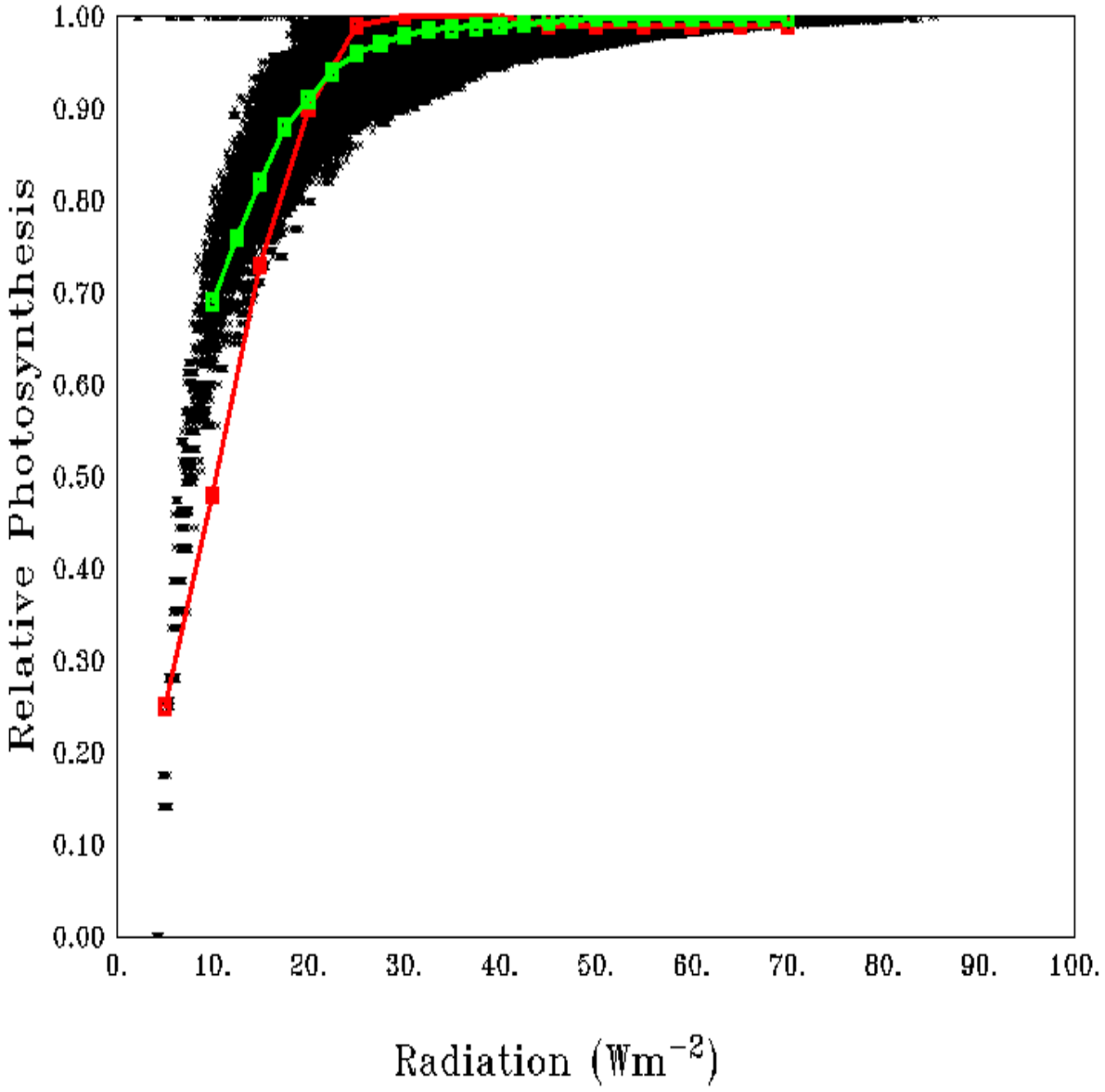

Figure 2: Scatter of average relative photosynthesis versus different light intensities in the model (black dots) and its mean (green curve). The red curve shows the theoretical P – I curve from Parsons et al., (1984).

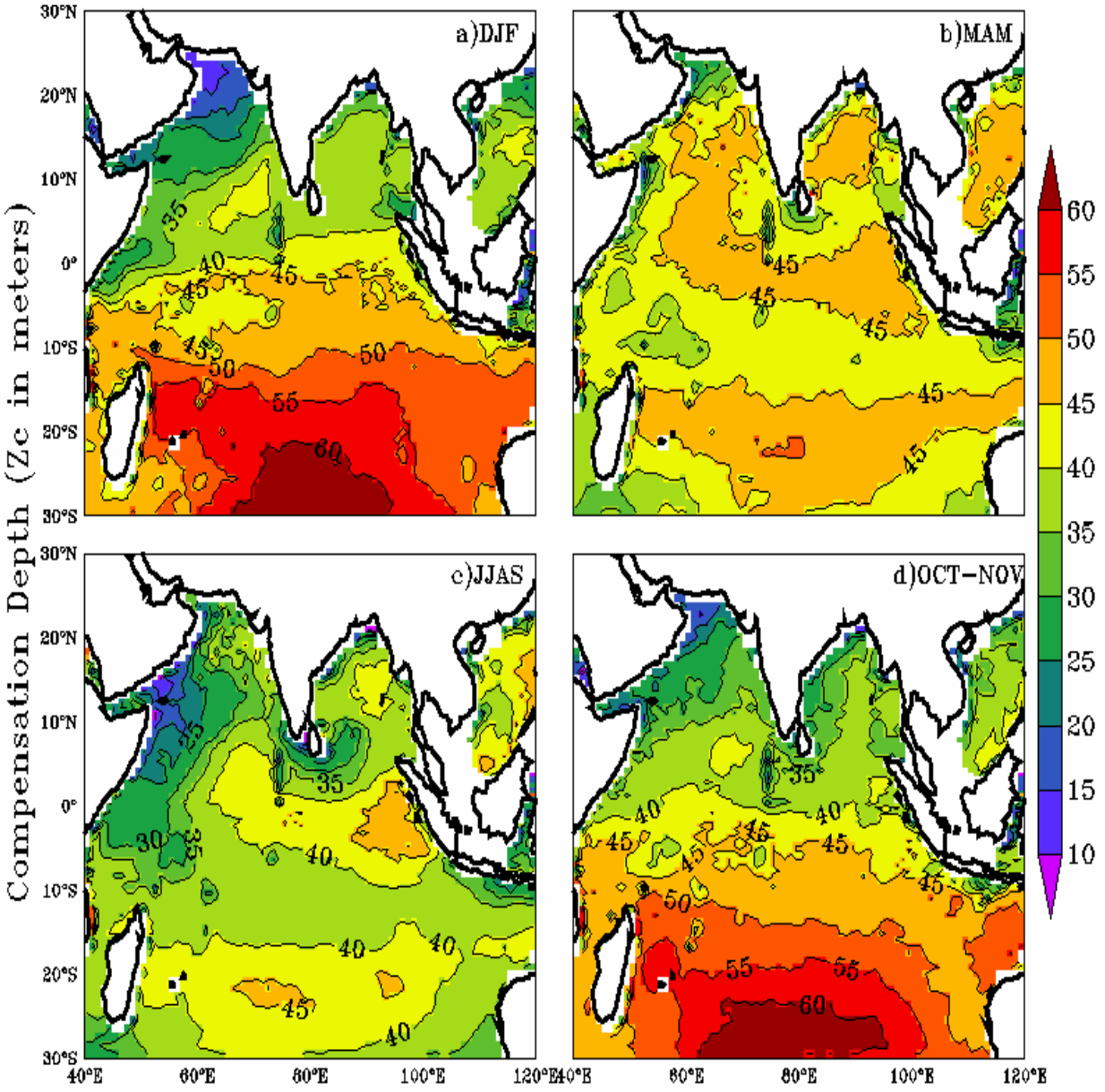

1055

1056 Figure 3: Seasonal-mean maps of varying compensation depth (varZc), (a) December to
1057 February (DJF), (b) March to May (MAM), (c) June to September (JJAS), (d) October to
1058 November (ON). Units are meters.

1059

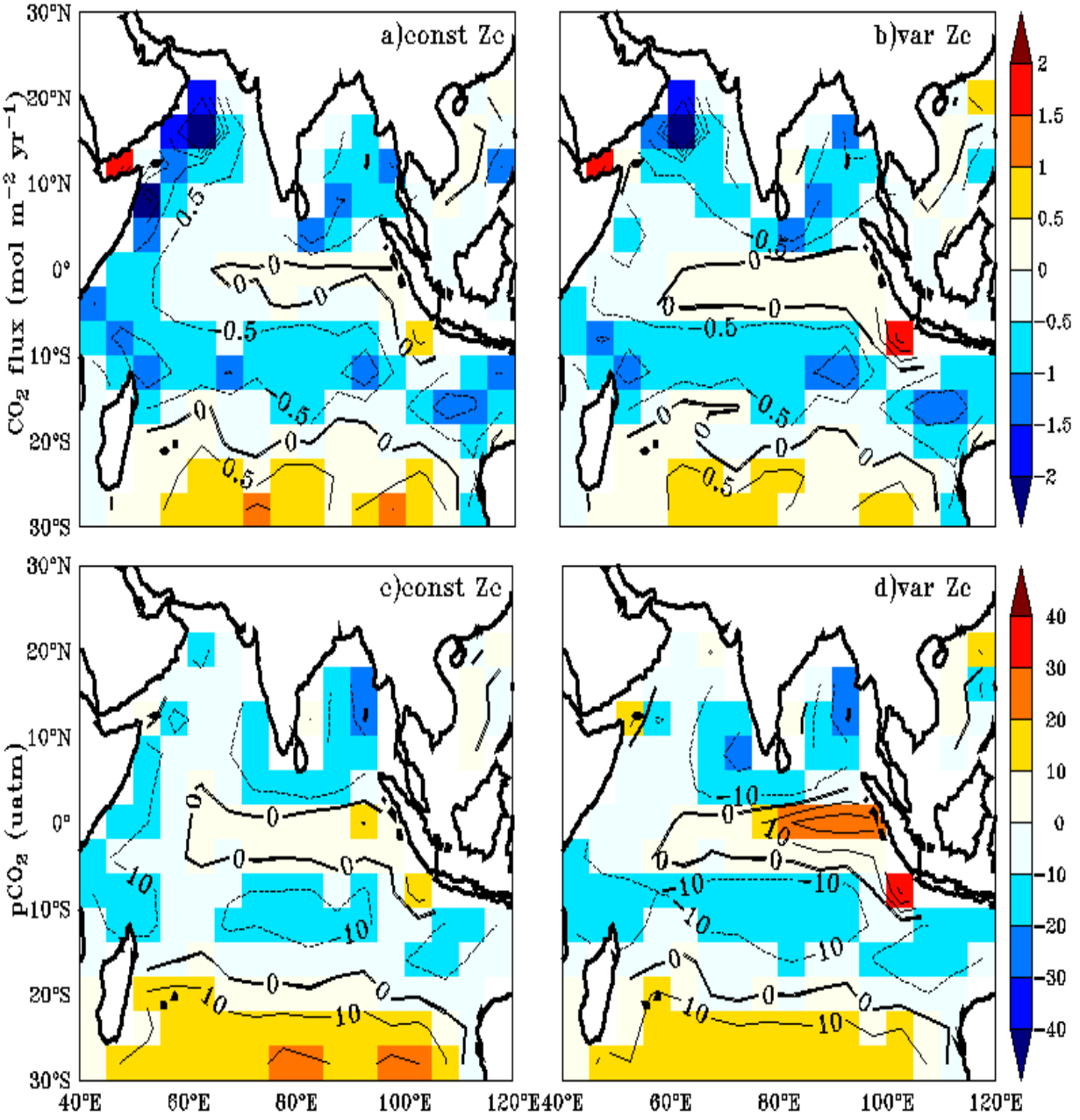

Figure 4: Annual mean biases in the model evaluated against Takahashi et al. (2009) observations for CO_2 flux (a, b) and pCO_2 (c, d) with constant Zc (constZc) and varying Zc (varZc). Units of CO_2 flux and pCO_2 are mol m^{-2} yr^{-1} and µatm, respectively.

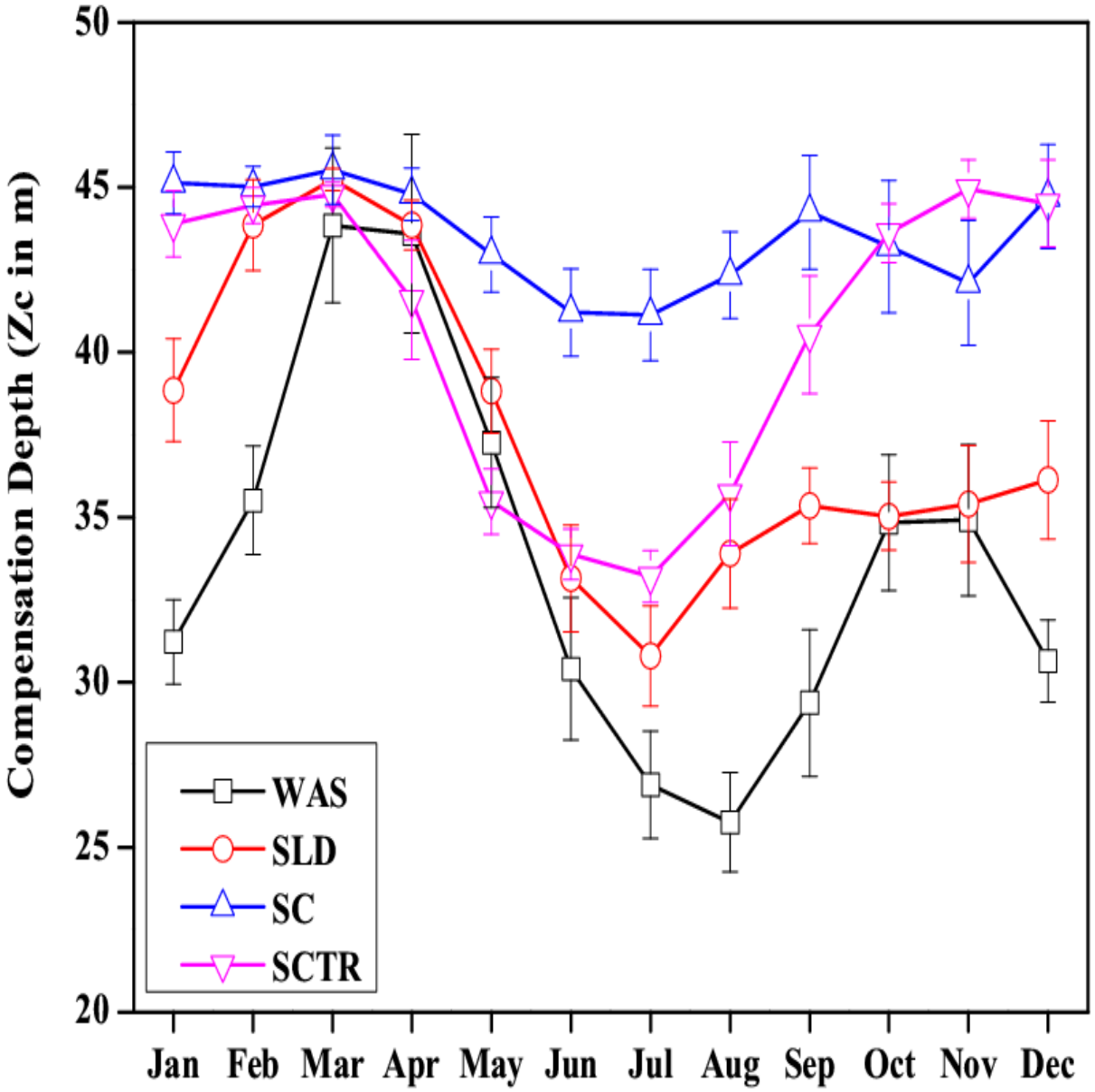

Figure 5: Seasonal variations in varZc over the study regions shown as climatology computed over 1990-2010. Error bar shows standard deviations of individual months over these years. Units are meters.

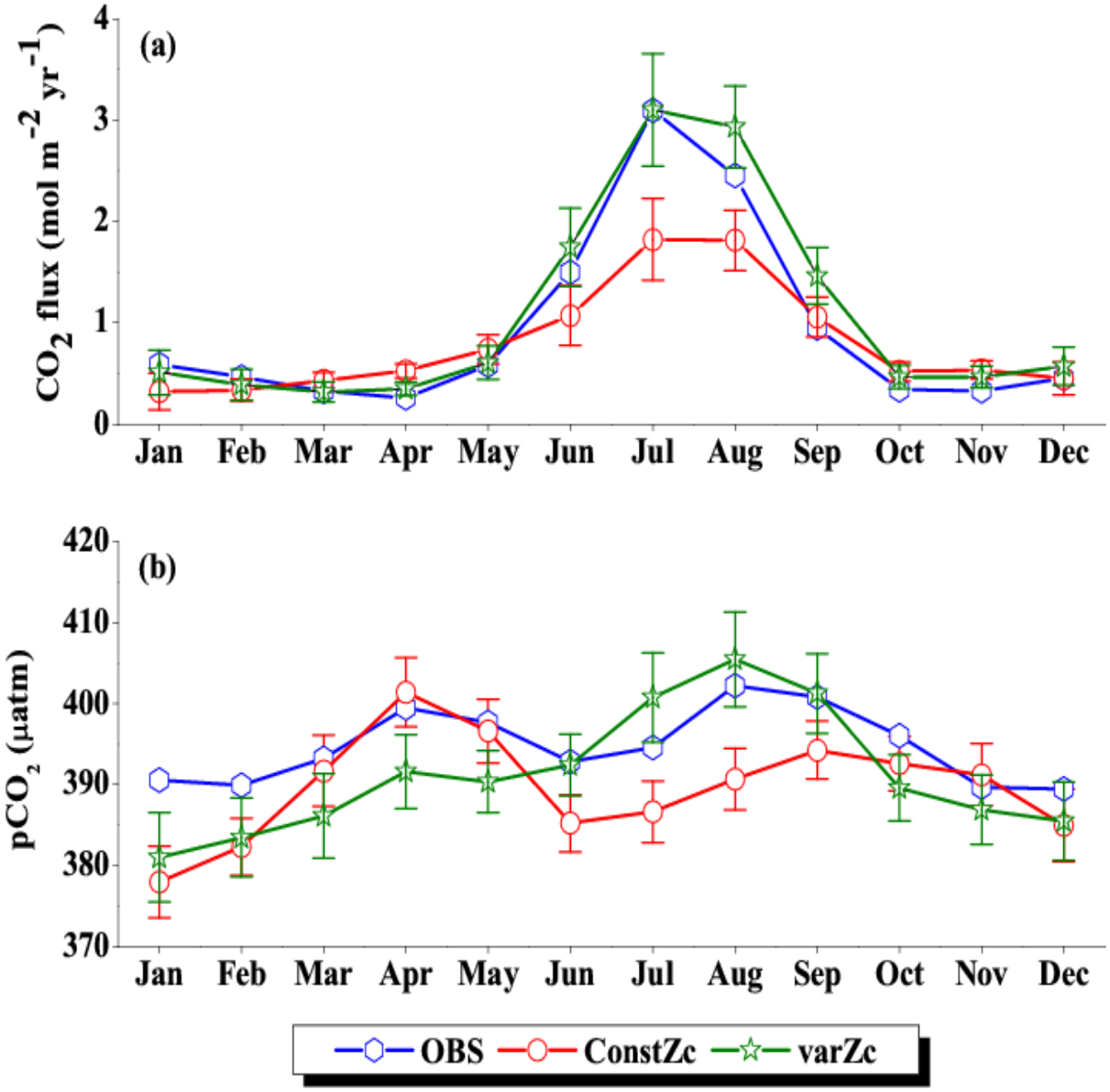

Figure 6: Comparison of model (a) CO_2 flux and (b) pCO_2 simulated with constZc and varZc with that of Takahashi et al. (2009) observations (OBS) over WAS as climatology computed over 1990-2010. Error bar shows standard deviations of individual months over these years. Units of CO_2 flux and pCO_2 are mol m^{-2} yr^{-1} and µatm, respectively. Legend is common for both graphs.

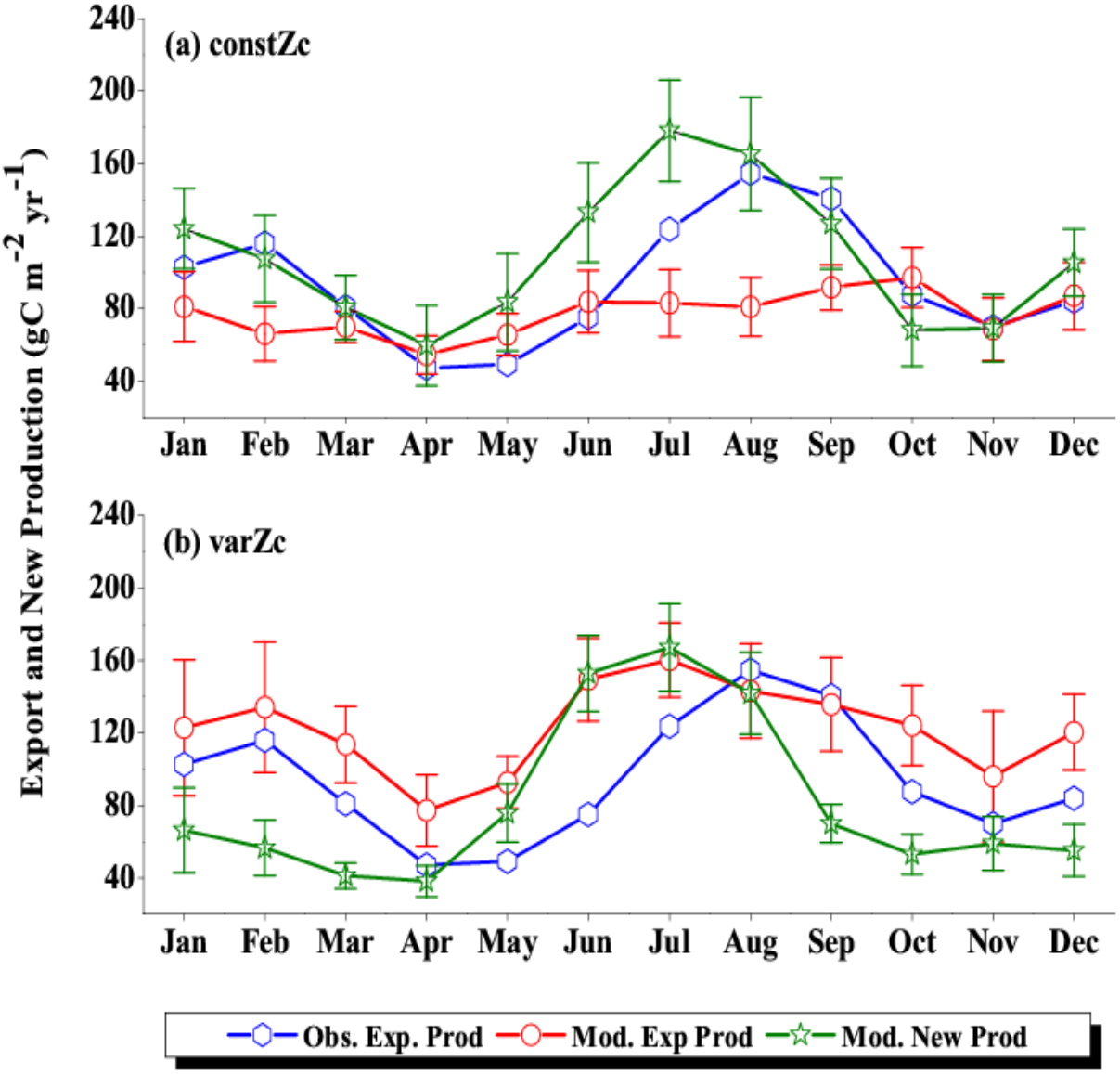

1074

1075 Figure 7: Comparison of model export production (Mod. Exp. Prod) and new production (Mod.
1076 New Prod) with satellite-derived export production (Obs. Exp. Prod) for (a) ConstZc and (b)
1077 varZc simulations for WAS. Units are g C m^{-2} yr^{-1}. Legends are common for both graphs.

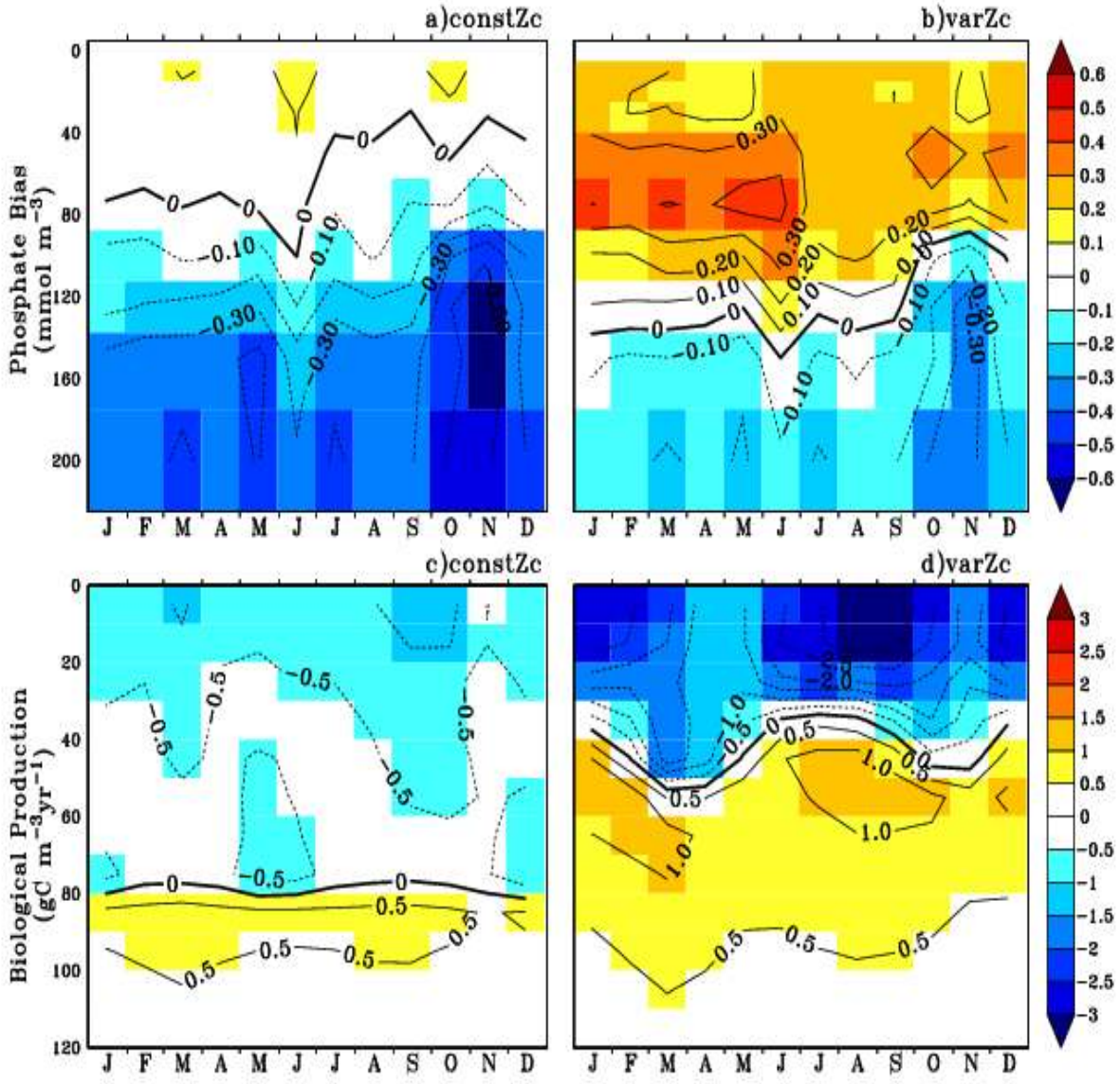

Figure 8: Annual mean bias of model phosphate when compared with climatological observational data (a) for constZc and (b) for varZc simulations. Corresponding annual mean biological source/sink profiles (c, d) in the model for WAS. Unit of phosphate is mmol m^{-3} and biological source/sink is g C m^{-3} yr^{-1}.

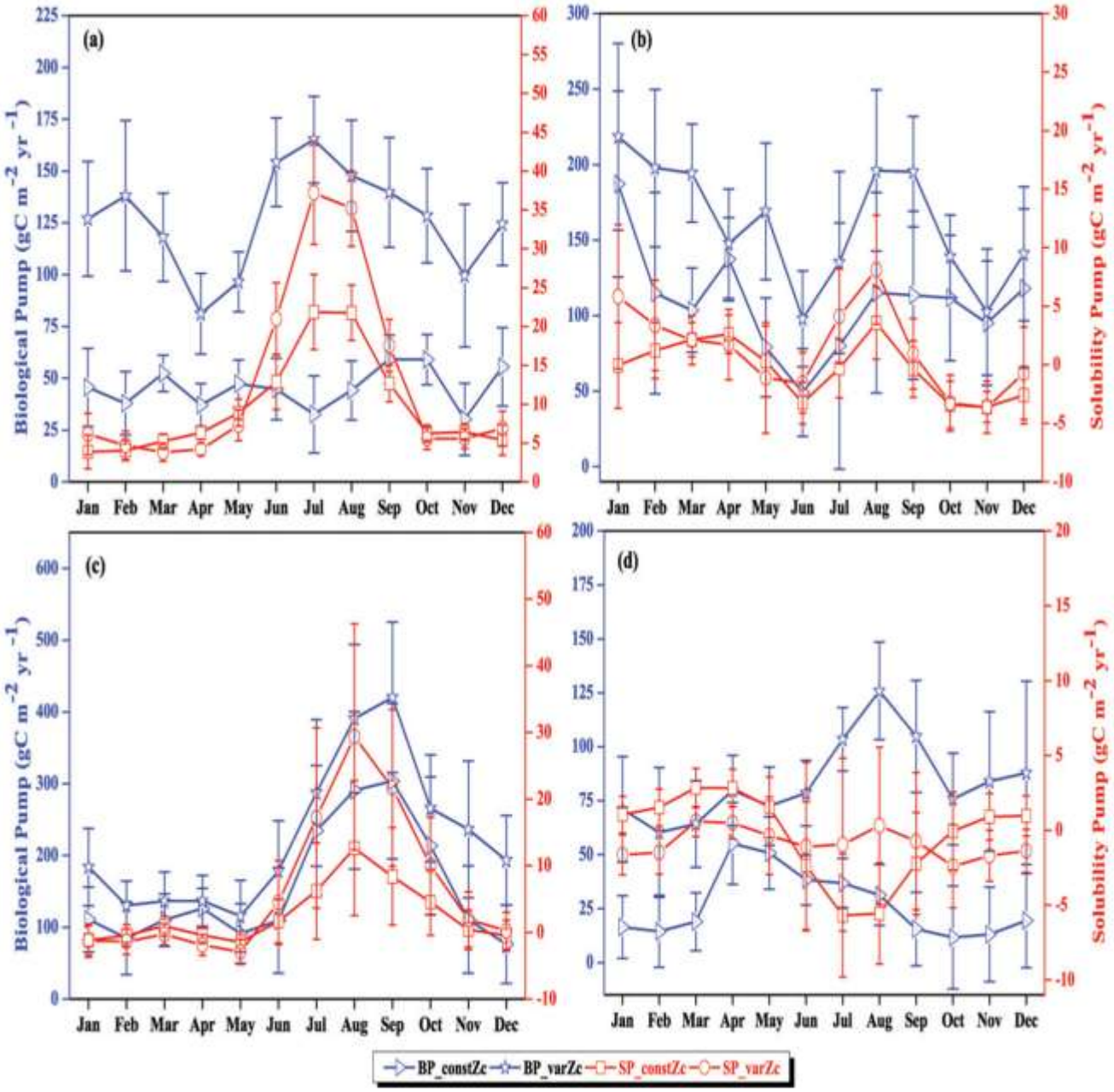

Figure 9: The strength of the biological pump (BP, black lines) and solubility pump (SP, red lines) from constZc and varZc simulations for (a) WAS (b) SLD (c) SC and (d) SCTR. The left axis shows the biological pump and the right axis shows the solubility pump. Error bar shows standard deviations of individual months over the years 1990 - 2010. Units are g C m^{-2} yr^{-1}.

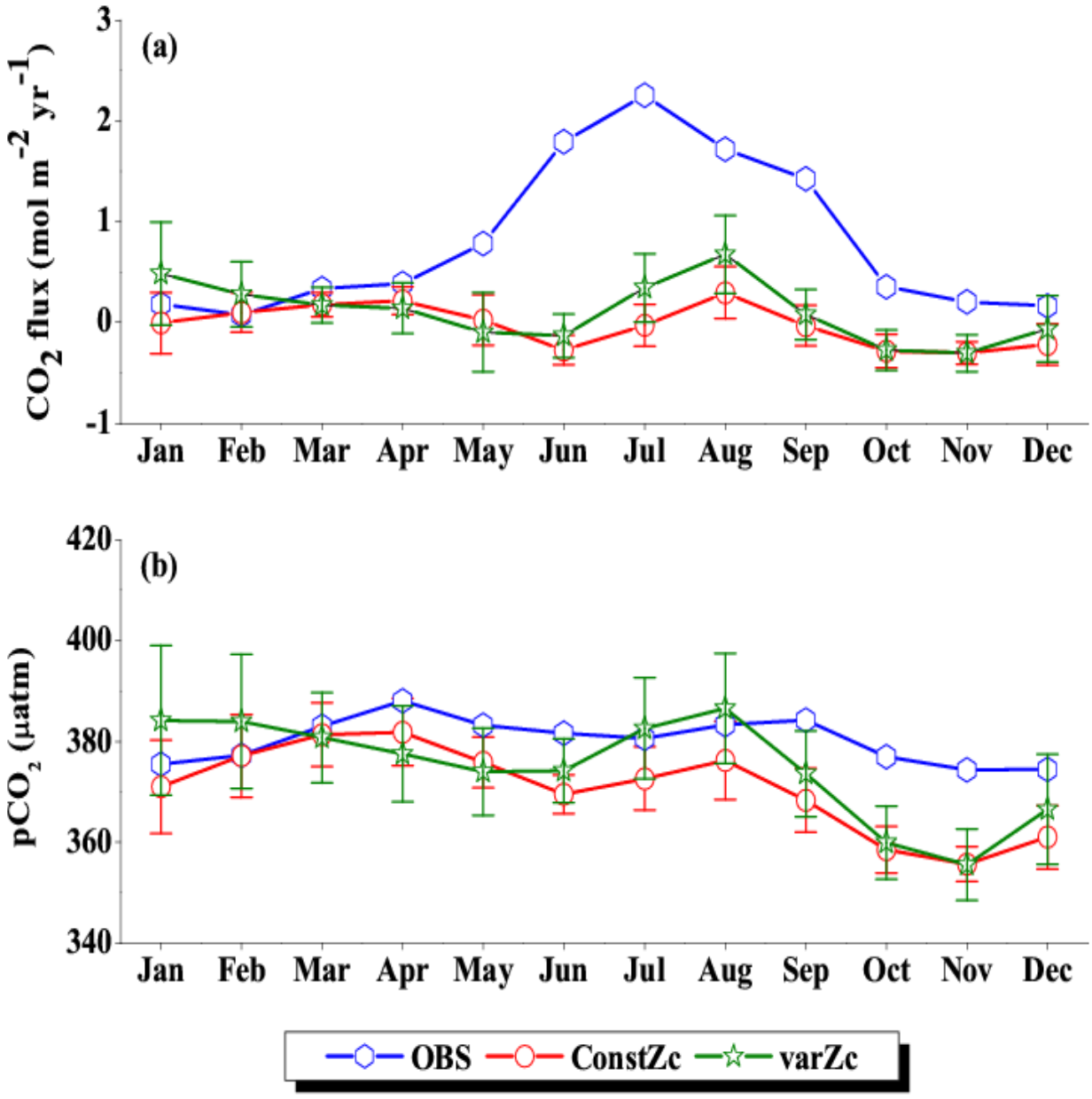

Figure 10: Same as Figure (6), but for SLD.

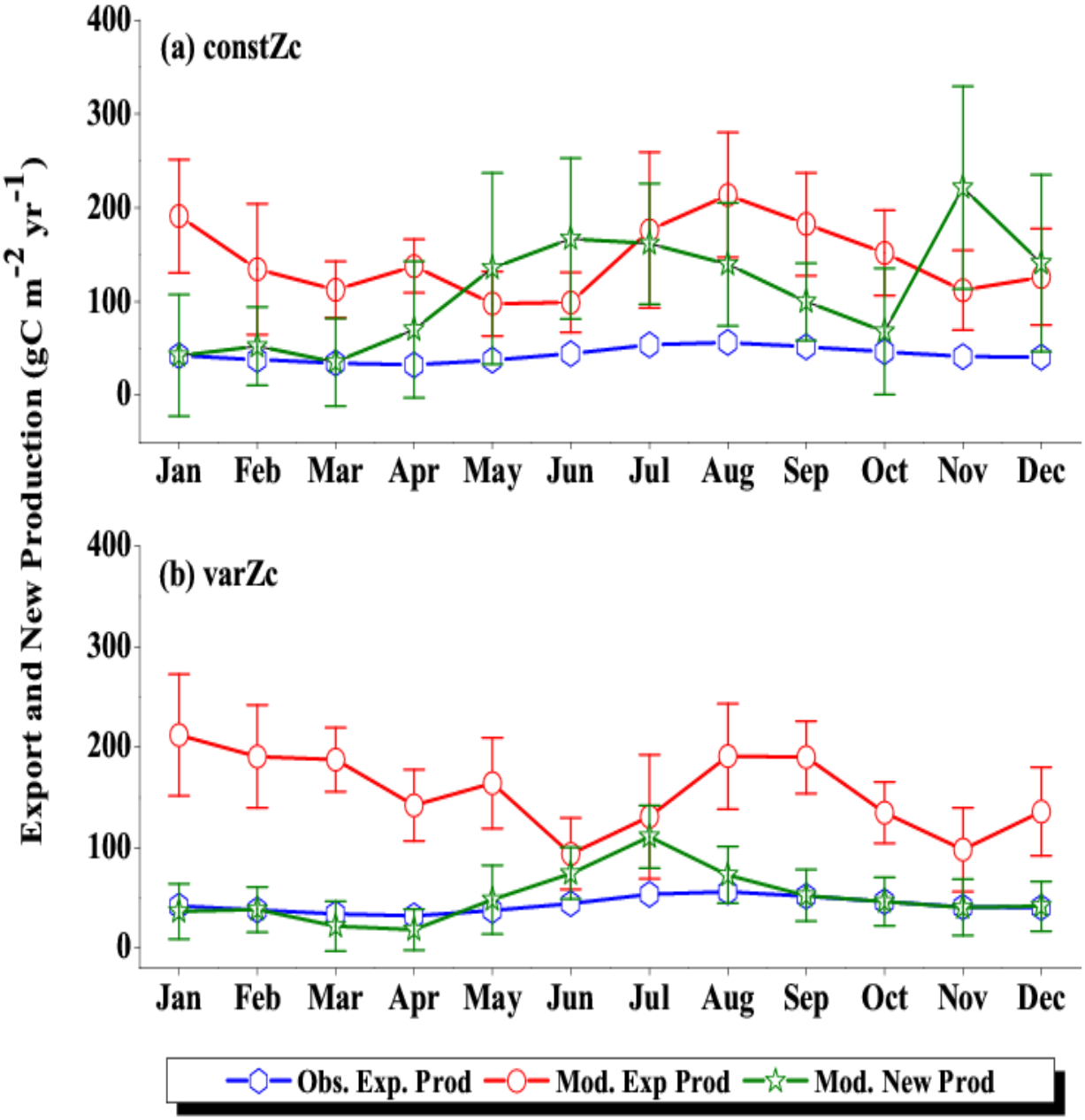

1094

1095 Figure 11: Same as Figure (7), but for SLD.

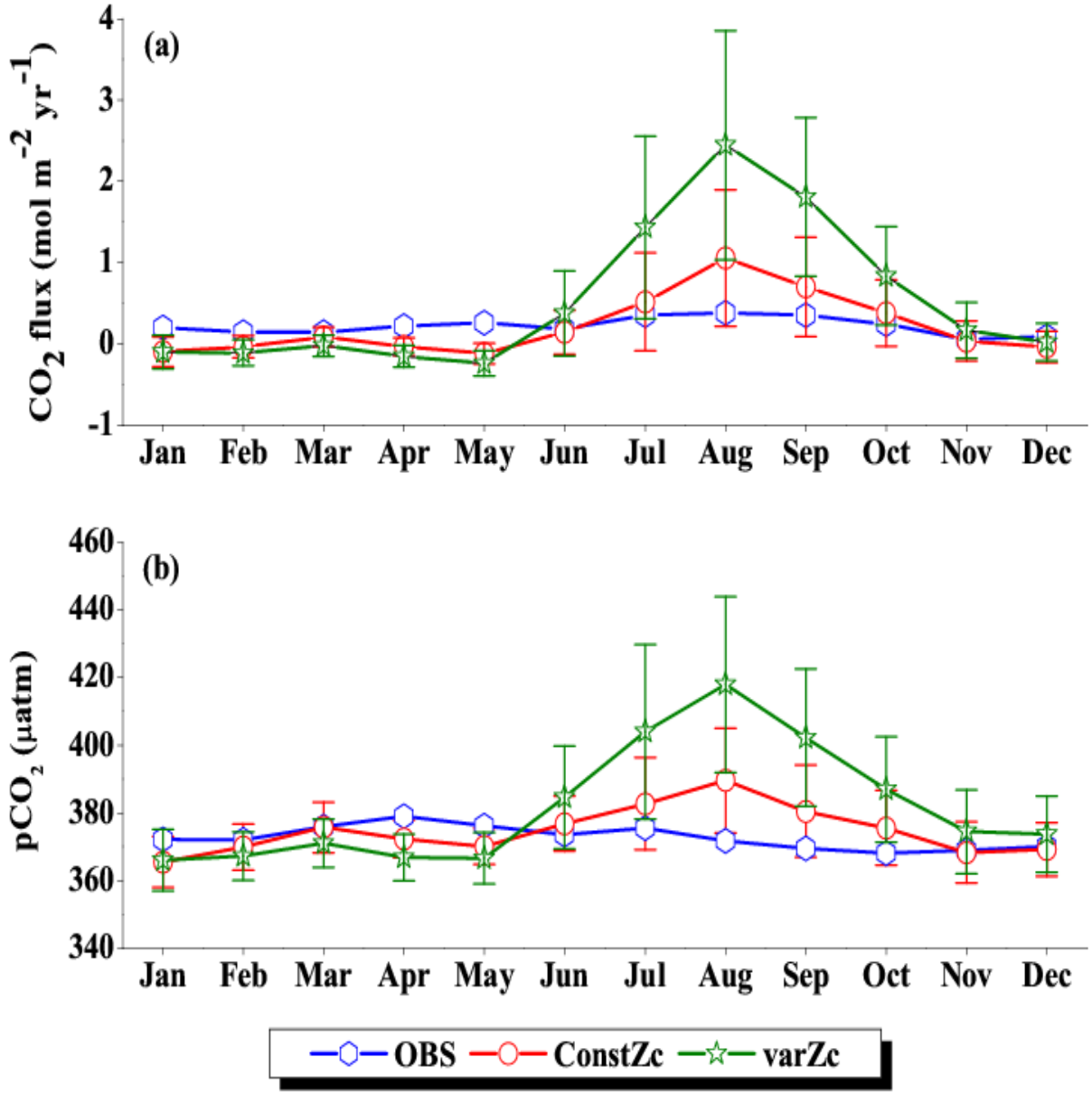

1096

1097 Figure 12: Same as Figure (6), but for SC.

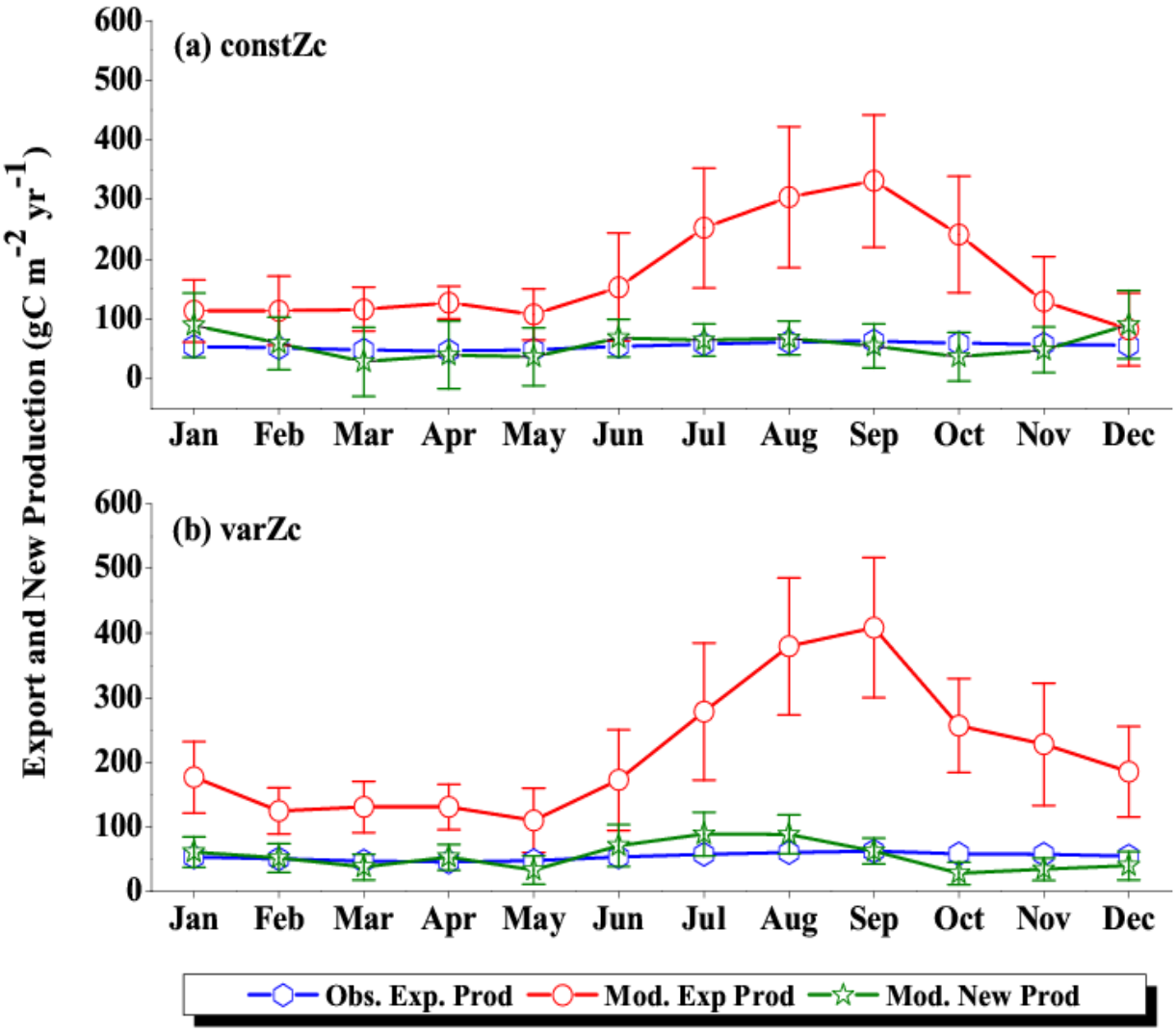

1098

1099 Figure 13: Same as Figure (7), but for SC.

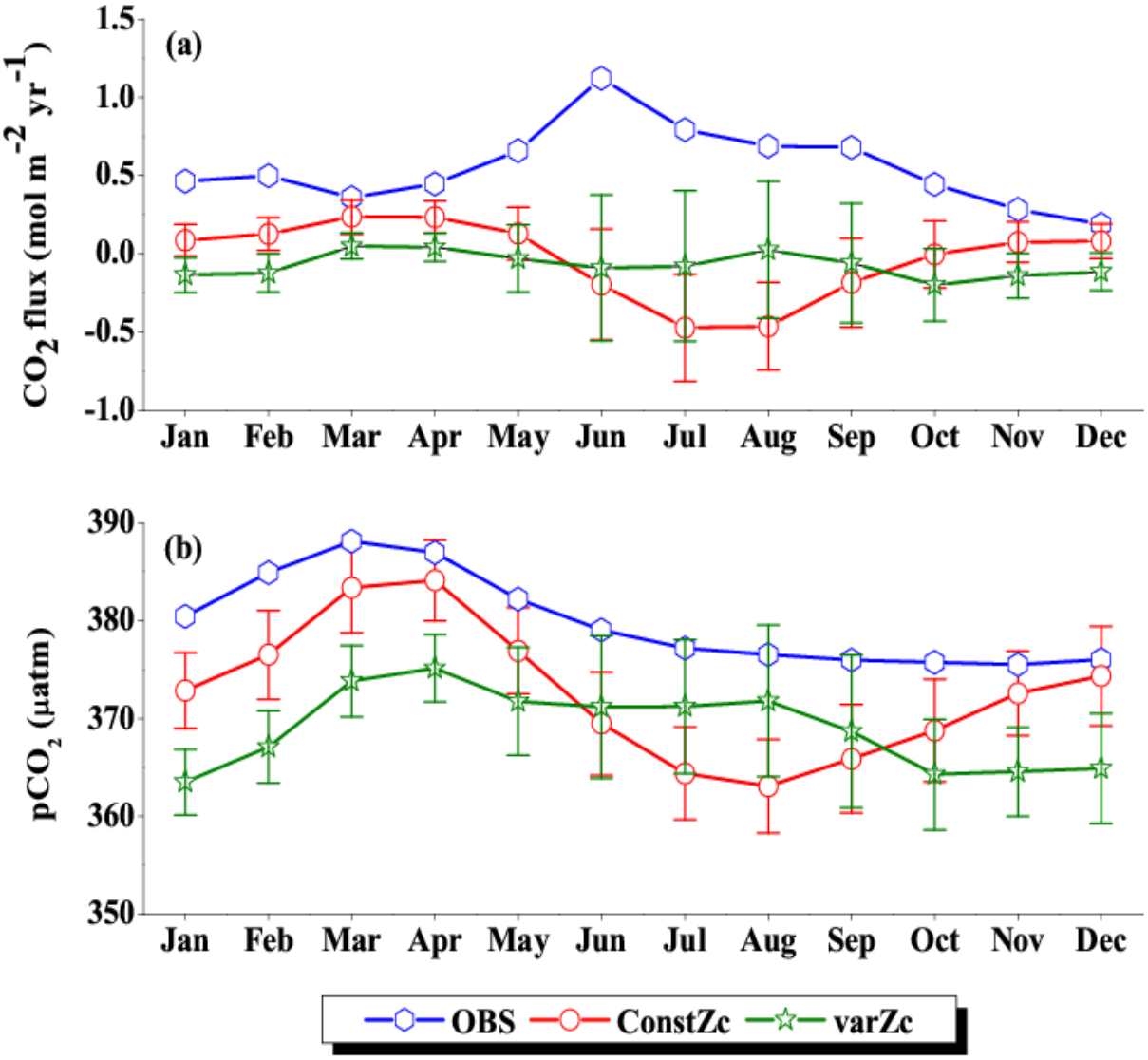

Figure 14: Same as Figure (6), but for SCTR.

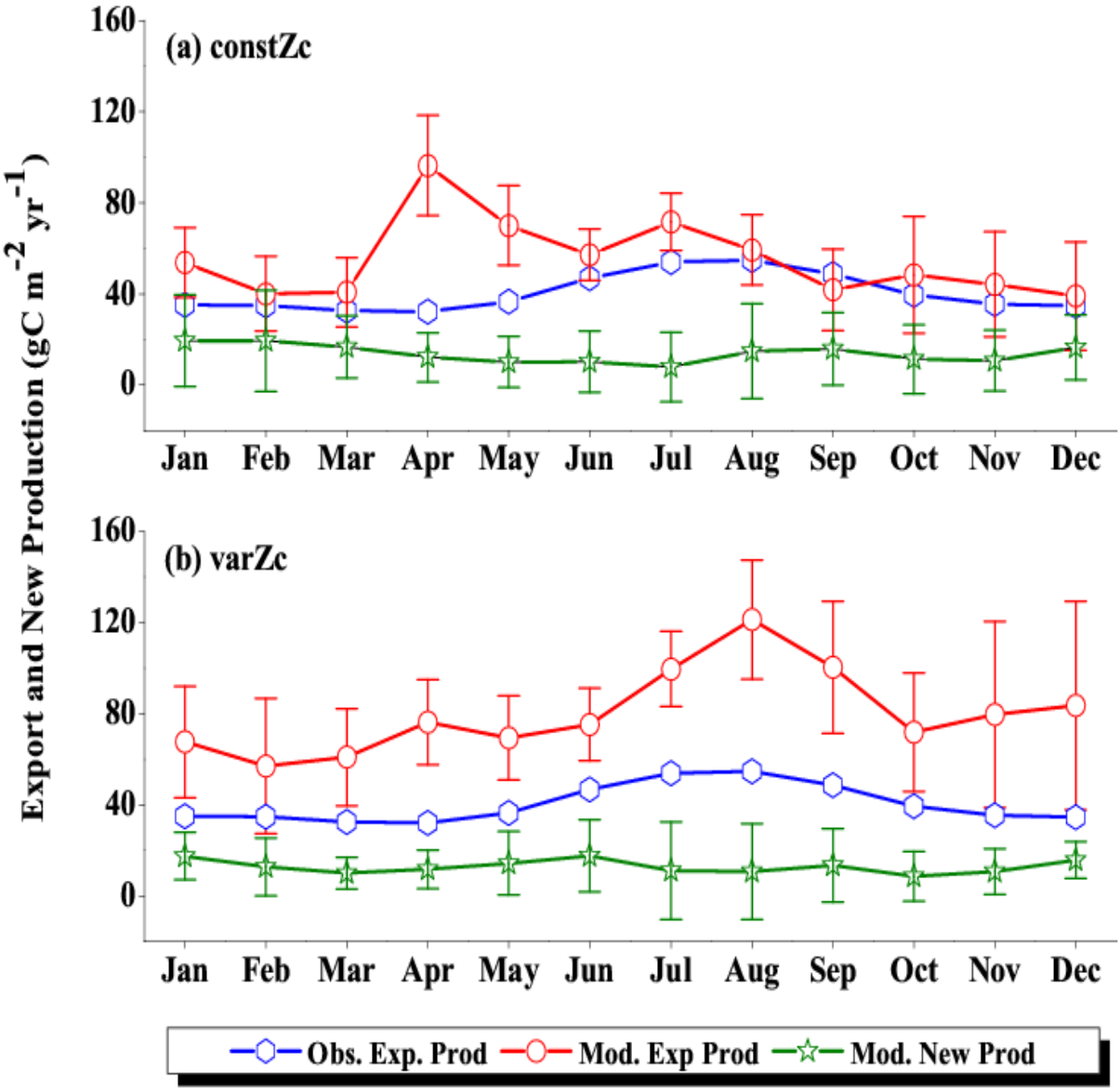

Figure 15: Same as Figure (7), but for SCTR.